Article

Molecular Cell

Continuous Histone Replacement by Hira Is Essential for Normal Transcriptional Regulation and De Novo DNA Methylation during Mouse Oogenesis

Graphical Abstract

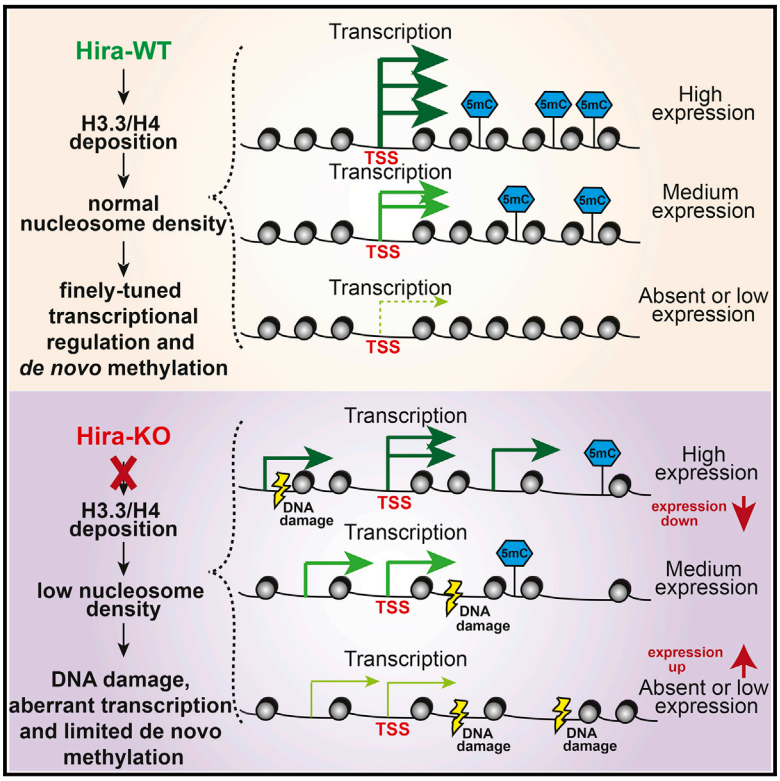

Authors

Buhe Nashun, Peter W.S. Hill, Sebastien A. Smallwood, ..., Richard J. Festenstein, Gavin Kelsey, Petra Hajkova

Correspondence

petra.hajkova@csc.mrc.ac.uk

In Brief

To address the extent to which basic cellular processes depend on replication-independent chromatin assembly in vivo, Nashun et al. deleted histone H3.3 chaperone *Hira* during mouse oogenesis. Their results demonstrate a critical relationship between continuing histone replacement, chromatin homeostasis, transcriptional regulation, and de novo DNA methylation.

Highlights

- Histone H3/H4 replacement is continuous and mediated by Hira during mouse oogenesis
- Loss of Hira results in chromatin abnormalities and extensive oocyte loss
- Hira depletion reduces histone load, which prevents normal transcriptional regulation
- Hira-mediated histone replacement is required for normal 5mC deposition in oocytes

Accession Numbers

GSE66931
GSE73382
GSE66629

Nashun et al., 2015, Molecular Cell *60*, 611–625
November 19, 2015 ©2015 The Authors
http://dx.doi.org/10.1016/j.molcel.2015.10.010

CrossMark

CellPress

Molecular Cell
Article

Continuous Histone Replacement by Hira Is Essential for Normal Transcriptional Regulation and De Novo DNA Methylation during Mouse Oogenesis

Buhe Nashun,[1] Peter W.S. Hill,[1] Sebastien A. Smallwood,[2] Gopuraja Dharmalingam,[1] Rachel Amouroux,[1] Stephen J. Clark,[2] Vineet Sharma,[1,3] Elodie Ndjetehe,[1] Pawel Pelczar,[4,6] Richard J. Festenstein,[1,3] Gavin Kelsey,[2,5] and Petra Hajkova[1,*]

[1]Medical Research Council Clinical Sciences Centre (MRC CSC), Faculty of Medicine, Imperial College London, London W12 0NN, UK
[2]Epigenetics Programme, The Babraham Institute, Cambridge CB22 3AT, UK
[3]Department of Medicine, Division of Brain Sciences, Faculty of Medicine, Imperial College London, London W12 0NN, UK
[4]Transgenic and Reproductive Techniques Laboratory, Institute of Laboratory Animal Science, University of Zurich, 8091 Zurich, Switzerland
[5]Centre for Trophoblast Research, University of Cambridge, Cambridge CB22 3AT, UK
[6]Present address: TMCF, University of Basel, Mattenstrasse 24a, 4058 Basel, Switzerland
*Correspondence: petra.hajkova@csc.mrc.ac.uk
http://dx.doi.org/10.1016/j.molcel.2015.10.010
This is an open access article under the CC BY-NC-ND license (http://creativecommons.org/licenses/by-nc-nd/4.0/).

SUMMARY

The integrity of chromatin, which provides a dynamic template for all DNA-related processes in eukaryotes, is maintained through replication-dependent and -independent assembly pathways. To address the role of histone deposition in the absence of DNA replication, we deleted the H3.3 chaperone *Hira* in developing mouse oocytes. We show that chromatin of non-replicative developing oocytes is dynamic and that lack of continuous H3.3/H4 deposition alters chromatin structure, resulting in increased DNase I sensitivity, the accumulation of DNA damage, and a severe fertility phenotype. On the molecular level, abnormal chromatin structure leads to a dramatic decrease in the dynamic range of gene expression, the appearance of spurious transcripts, and inefficient de novo DNA methylation. Our study thus unequivocally shows the importance of continuous histone replacement and chromatin homeostasis for transcriptional regulation and normal developmental progression in a non-replicative system in vivo.

INTRODUCTION

DNA in all eukaryotic organisms is bound by nucleosomes, forming a physiological chromatin context in which all molecular processes involving DNA operate. The integrity of the chromatin template is constantly compromised by fundamental biological processes, such as DNA replication, repair, and transcription, following which the normal chromatin structure is restored with the help of histone chaperone proteins (Gurard-Levin et al., 2014; Ransom et al., 2010). Advances in recent years have shed light on some of the molecular players involved in chromatin assembly and maintenance, separating (on the molecular level) DNA replication-dependent and -independent pathways (Burgess and Zhang, 2013). Histone proteins themselves are central to these processes: the expression and incorporation of canonical histones is tightly coupled to DNA replication; in contrast, histone variants can be incorporated into chromatin independent of the cell cycle (Maze et al., 2014).

While it has become increasingly clear that the activity of histone chaperone proteins is of critical importance during DNA replication and repair (Adam et al., 2013; Hoek and Stillman, 2003; Polo et al., 2006; Ransom et al., 2010), studies that have attempted to dissect the importance of histone replacement in the interphase nucleus have revealed only a limited contribution of histone chaperones and/or variants to transcriptional regulation (Banaszynski et al., 2013; Goldberg et al., 2010; Hödl and Basler, 2009; Sakai et al., 2009). These studies, however, have been complicated by the use of proliferative cell systems that could (at least partially) restore chromatin integrity through replication-coupled chromatin assembly (Banaszynski et al., 2013; Hödl and Basler, 2009; Sakai et al., 2009; Wyrick et al., 1999). Thus, the extent to which basic physiological processes, such as transcription, are dependent on or regulated by histone replacement remains unclear.

To overcome the limitations of these previous studies, we took advantage of the unique system presented by mammalian oogenesis. Over an extended time span and in the absence of DNA replication, postnatal mammalian oocytes execute the oogenesis-specific developmental program, involving widespread transcriptional changes and de novo DNA methylation, ultimately acquiring the competencies required for fertilization and embryogenesis (De La Fuente, 2006; Li and Albertini, 2013; Tomizawa et al., 2012).

To address the importance of histone turnover during this process, we have generated a mouse oocyte-specific knockout of the histone chaperone *Hira*. As opposed to Caf1, which is implicated in the replication-coupled deposition of canonical histones H3.1 and H3.2, Hira has been shown to deposit the H3.3 variant during replication-independent chromatin assembly (Ray-Gallet

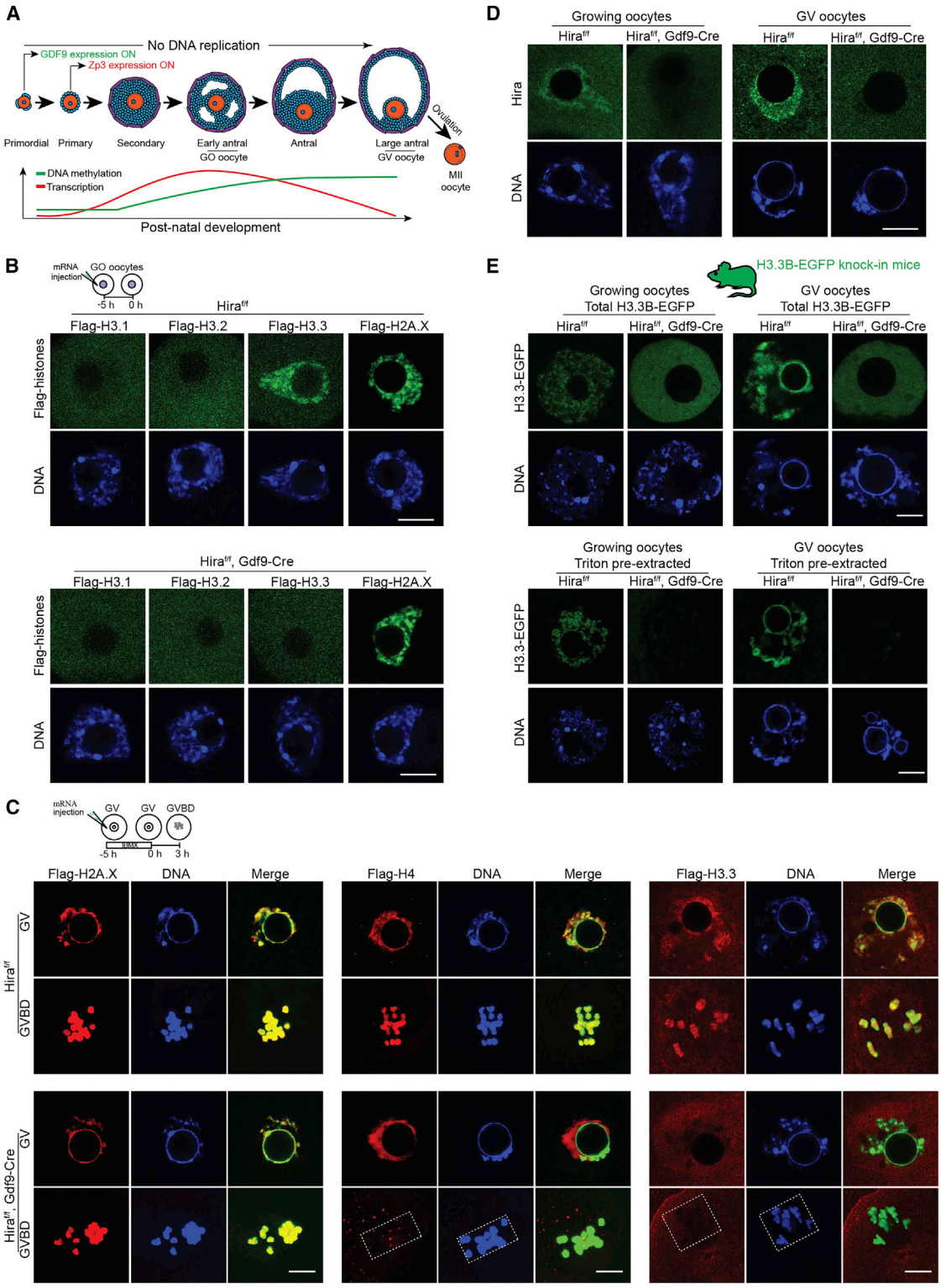

Figure 1. Incorporation of H3.3 in Developing Oocytes Is Driven by Hira

(A) Schematic illustration shows developmental stages and global transcriptional activity during oogenesis with indicated onset of *Gdf9-Cre*$^{+}$ and *Zp3-Cre*$^{+}$ expression (adapted from De La Fuente, 2006; Lan et al., 2004; Li and Albertini, 2013; and Tomizawa et al., 2012).

(B) Growing oocytes (postnatal day [P]14) were subjected to mRNA microinjection of Flag-tagged H3.1, H3.2, H3.3, or H2A.X. Incorporation of histone variants was visualized by anti-Flag antibody staining.

(legend continued on next page)

et al., 2002; Tagami et al., 2004). Our findings show that depletion of Hira in primordial oocytes causes a severe developmental defect associated with extensive oocyte death. On the molecular level, Hira depletion compromises the oocyte's ability to replace histones H3 and H4. This causes significantly increased DNA accessibility, accumulation of DNA damage, and chromosome segregation defects. The lack of normal chromatin structure has a striking impact on transcriptional regulation: lack of normal H3.3/H4 replacement prevents the oocytes from maintaining full dynamic range of gene expression, and it leads to compromised transcriptional transitions normally associated with the oocyte development. Furthermore, we show that histone replacement is necessary for silencing of spurious transcription and, in the context of the oocyte, also for the efficient deposition of de novo DNA methylation.

Our results thus uniquely demonstrate the critical relationship between continuous histone replacement, the structural integrity of the chromatin template, the normal regulation of transcription, and the establishment of DNA methylation, in the context of an in vivo developmental system.

RESULTS

Hira Is Responsible for H3.3/H4 Turnover in Postnatal Oocytes

In the mouse, female germ cells arrest in prophase of the first meiotic division at embryonic day (E)13.5. The female gonocytes subsequently resume growth in postnatal ovaries where they undergo oogenesis and progress through meiosis (De La Fuente, 2006). This process involves the following: (1) pronounced transcriptional changes as the developing oocytes progress from primordial to large antral follicle stages; (2) the deposition of de novo DNA methylation starting in the secondary follicle stage; (3) the silencing of transcription in the germinal vesicle (GV) stage; and, finally, (4) the condensation of chromosomes in the MII stage, resulting in an oocyte that is competent to undergo fertilization and support early embryonic development (Figure 1A).

We first addressed the capacity of developing oocytes to incorporate histones by microinjection of mRNA for tagged versions of histones. In agreement with the absence of replication during oocyte maturation, growing oocytes did not show any incorporation of canonical histones H3.1 and H3.2 (Figure 1B; Akiyama et al., 2011). In contrast, microinjected Flag-tagged H3.3 and H2A.X, previously shown to be enriched in the developing oocyte (Akiyama et al., 2011; Nashun et al., 2010), were readily incorporated into the chromatin of growing oocytes (Figure 1B). We thus conclude that H3.3 is the only H3 subtype incorporated during postnatal oocyte development. In further support of this observation, oocytes isolated from our H3.3B-EGFP knockin mice (Figure S1G) confirmed that both growing and GV oocytes contain high levels of nuclear H3.3 (Figure 1E). Growing oocytes are transcriptionally highly active, which could explain the observed histone turnover. However, we also detected a high level of chromatin incorporation for Flag-tagged H2A.X, H4, and H3.3 upon injection of tagged histone mRNA into transcriptionally inactive GV-stage oocytes (Figure 1C), demonstrating that the chromatin in the mature GV oocyte is still dynamic even after global transcription has ceased.

Previous studies have shown that the majority of H3.3 incorporation is critically dependent on the presence of histone chaperone Hira (Goldberg et al., 2010; Pchelintsev et al., 2013). In agreement with the observed H3.3 incorporation, Hira is expressed and shows nuclear localization during postnatal oocyte development (Figure 1D). To investigate whether Hira is specifically required for the observed H3.3 incorporation during oogenesis, we took advantage of *Gdf9*- and *Zp3*-driven expression of Cre recombinase and deleted *Hira* in the primordial and primary stages of follicle development, respectively (Figures 1A and S1A). We confirmed that both *Gdf9-Cre*- and *Zp3-Cre*-deleted oocytes undergo genetic recombination (Figure S1B; data not shown) and are depleted of *Hira* mRNA, protein and complex (Figures 1D and S1C–S1F).

The absence of Hira severely decreased H3.3 content and completely abolished the incorporation of microinjected tagged H3.3 in both growing and GV-stage oocytes (Figures 1B, 1C, and 1E). The observed impairment of H3.3 incorporation occurred despite the presence of an alternative ATRX/DAXX chaperone complex that has been well characterized to incorporate H3.3 (Burgess and Zhang, 2013; Maze et al., 2014). Of note, the presence and the localization of this complex in the GV oocyte were not affected by *Hira* deletion (Figure S2A), and we could observe H3.3B-EGFP loci overlapping with ATRX staining in $Hira^{f/f}$ *Gdf9-Cre*$^{+}$, H3.3B-EGFP GV oocytes at higher laser detection intensity (Figure S2C). The severe reduction of H3.3 incorporation in $Hira^{f/f}$ *Gdf9-Cre*$^{+}$ oocytes thus demonstrates that the ATRX/DAXX chaperone complex cannot compensate for the lack of Hira, as was also observed in mouse embryonic stem cells (ESCs) (Goldberg et al., 2010). The lack of Hira and H3.3 incorporation also was not compensated for by incorporation of the canonical histones H3.1 or H3.2 (Figure 1B), and it coincided with the lack of detectable incorporation of histone H4 (Figure 1C).

Taken together, these findings demonstrate that the histone variant H3.3, rather than H3.1 or H3.2, is actively incorporated into chromatin during oocyte development, and confirm that Hira is responsible for the incorporation of the majority of

(C) Flag-H2A.X, Flag-H4, and Flag-H3.3 mRNA was microinjected into the cytoplasm of transcriptionally inert GV oocytes from $Hira^{f/f}$ or $Hira^{f/f}$ *Gdf9-Cre*$^{+}$ siblings. Following 5-hr incubation in the IBMX-containing medium, the oocytes were either fixed (GV) or transferred to IBMX-free medium to induce germinal vesicle breakdown (GVBD) and the incorporation of tagged histones was visualized as in (B). Dashed rectangles indicate the location of condensed chromosomes of the GVBD oocyte.

(D) Lack of Hira in growing (P14, left) or GV-stage (GV, right) oocytes from $Hira^{f/f}$ *Gdf9-Cre*$^{+}$ is shown ($Hira^{f/f}$ siblings were used as controls).

(E) Deletion of Hira leads to dramatically reduced H3.3 in chromatin. Growing and GV oocytes from $Hira^{f/f}$, *H3.3B-EGFP*, or $Hira^{f/f}$ *Gdf9-Cre*$^{+}$, *H3.3B-EGFP* mice. (Top) Oocytes were subject to paraformaldehyde (PFA) fixation directly after collection. (Bottom) Oocytes were pre-extracted by Triton X-100 prior to PFA fixation to reveal chromatin-associated H3.3. A minimum of 12 oocytes were examined. DNA was stained with DAPI (in blue). Scale bar, 10 μm. See also Figures S1 and S2.

H3.3 in conjunction with histone H4 (Figures 1B–1E and S2B). Of note, although Hira-deficient oocytes failed to incorporate tagged H3 and H4 histones, the incorporation of tagged H2A.X was readily detectable (Figures 1B and 1C), confirming that distinct molecular pathways are implicated in the deposition of H3/H4 and H2A/H2B histones (Burgess and Zhang, 2013).

Hira Depletion Results in a Severe Ovarian Phenotype, Associated with Extensive Oocyte Death and the Failure to Support Zygotic Reprogramming or Embryonic Development

Assessment of females with oocyte-specific *Hira* deletion revealed that loss of Hira led to a severe ovarian phenotype. Significantly lower numbers of MII oocytes could be recovered following superovulation (Figure 2A); *Zp3-Cre*-driven deletion of *Hira* led to a more than 50% reduction in the number of ovulated MII oocytes, and this effect was even more dramatic upon earlier *Gdf9-Cre*-driven deletion (Figure 2A). Furthermore, GV oocytes (Figure 1A) isolated from both $Hira^{f/f}$ *Zp3-Cre*$^{+}$ and $Hira^{f/f}$ *Gdf9-Cre*$^{+}$ ovaries showed dramatically reduced competency to complete the GV-to-MII transition during in vitro maturation (Figure S2E).

The severity of *Hira* deletion was particularly obvious upon *Gdf9-Cre*-driven knockout. $Hira^{f/f}$ *Gdf9-Cre*$^{+}$ ovaries were significantly smaller (Figures 2B and S2F); and, although we could recover some GV oocytes from 3-week-old females, the ovaries of older mice contained only very few oocytes, which were predominantly at early developmental stages (Figures 2C and S2G). Further analysis of the superovulated $Hira^{f/f}$ *Gdf9-Cre*$^{+}$ MII oocytes revealed frequent defects in chromosome alignment and segregation and instances of aberrant polar body extrusion (Figure 2D).

In line with a severe ovarian phenotype and in agreement with recently published reports (Inoue and Zhang, 2014; Lin et al., 2014; Loppin et al., 2005), the surviving Hira-depleted oocytes were unable to either reprogram the paternal pronucleus or support early embryonic development after fertilization. In agreement with the observed enrichment of H3.3 and Hira in the paternal pronucleus of control zygotes (Figures S3A–S3C), fertilized $Hira^{f/f}$ *Gdf9-Cre*$^{+}$ oocytes could not fully de-condense the male pronucleus (Figure S3D), incorporate H3.3 (Figure S3E), or support normal zygotic development (Figure S3F). Failure to incorporate H3.3 occurred despite the efficient removal of protamines (Figure S4A), indicating that protamine removal and chromatinization of the paternal genome are mechanistically distinct (Inoue and Zhang, 2014; Lin et al., 2014). Although the histone load of the paternal pronucleus was severely reduced upon maternal Hira deletion, we could detect a residual amount of histones on the paternal DNA by immunofluourescent staining (Figure S4B). However, it remains to be addressed whether the residual histones were inherited from sperm or whether they were incorporated in a Hira-independent manner. In agreement with the severe chromatinization defect, the partially decondensed paternal pronucleus of zygotes in which *Hira* had been maternally deleted failed to undergo DNA demethylation (Figure S4C) and could not provide a normal template for zygotic replication or transcription (Figures S4D and S4E; Lin et al., 2014).

Apart from the failure to support normal reprogramming of the paternal pronucleus following fertilization, Hira-depleted oocytes showed severe maternal defects. The ATP content was significantly reduced in Hira-depleted MII oocytes (Figure S2H), and, upon parthenogenetic activation, only a fraction of these oocytes reached the two-cell stage and none progressed further, contrary to the control oocytes that efficiently supported development of parthenogenetic blastocysts (Figure 2E).

Hira-Depleted Oocytes Show Increased DNA Accessibility and Accumulation of DNA Damage

Considering the pronounced oocyte phenotype, we set out to understand the molecular mechanisms by which Hira regulates oocyte development. We hypothesized that, in the absence of H3/H4 incorporation, the chromatin structure in Hira-depleted oocytes would be severely affected. In agreement with this, the histone content of Hira-depleted GV-stage oocytes was severely reduced (Figures 3A and S2B), and the resulting chromatin displayed altered structure and increased DNase I sensitivity (Figures 3B and 3C). Moreover, in accordance with the predicted role of histones in protecting genetic material from environmental stress and mutagenesis (Ljungman and Hanawalt, 1992), Hira-depleted oocytes showed clear signs of DNA damage both by increased levels of γ-H2AX (Figure 3D) and upregulation of DNA damage-responsive genes (Figure 3E).

Continuing Histone Replacement Mediated by Hira Is Required to Maintain the Full Dynamic Range of Gene Expression

The importance of Hira and continuous H3.3 replacement has been previously assessed in the context of proliferating mouse pluripotent ESCs (Banaszynski et al., 2013; Goldberg et al., 2010). These studies surprisingly revealed that Hira deletion led to only minor transcriptional changes (Banaszynski et al., 2013; Goldberg et al., 2010). Considering the severity of the phenotype observed following the deletion of Hira in oocytes, we next asked whether the reduced H3/H4 incorporation and increased DNA accessibility (Figures 1B–1E, 3A, and 3C) affected the transcriptional program of the Hira-depleted oocytes. Surprisingly, although the lack of maternal Hira severely affected the amount of transcription emanating from the paternal pronucleus following fertilization (Figure S4E; Lin et al., 2014), Hira-depleted and control growing oocytes showed similar global levels of transcription, as judged by EU incorporation (Figure 4A).

To address the role of Hira in transcription during oocyte development in depth, we carried out single-cell RNA sequencing (scRNA-seq) on four $Hira^{f/f}$ *Gdf9-Cre*$^{+}$ and four $Hira^{f/f}$ control oocytes. We chose to analyze ovulated MII oocytes that had successfully completed their first meiotic division to avoid inconsistencies due to differences in staging or developmental progression. Of note, consistent with the identical patterns of EU incorporation in the $Hira^{f/f}$ *Gdf9-Cre*$^{+}$ and control growing oocytes (Figure 4A), normalization to the ERCC RNA spike-ins included in our scRNA-seq library preparations revealed no significant differences in the total quantity of poly-adenylated RNA between $Hira^{f/f}$ *Gdf9-Cre*$^{+}$ and control MII oocytes (Figure 4B).

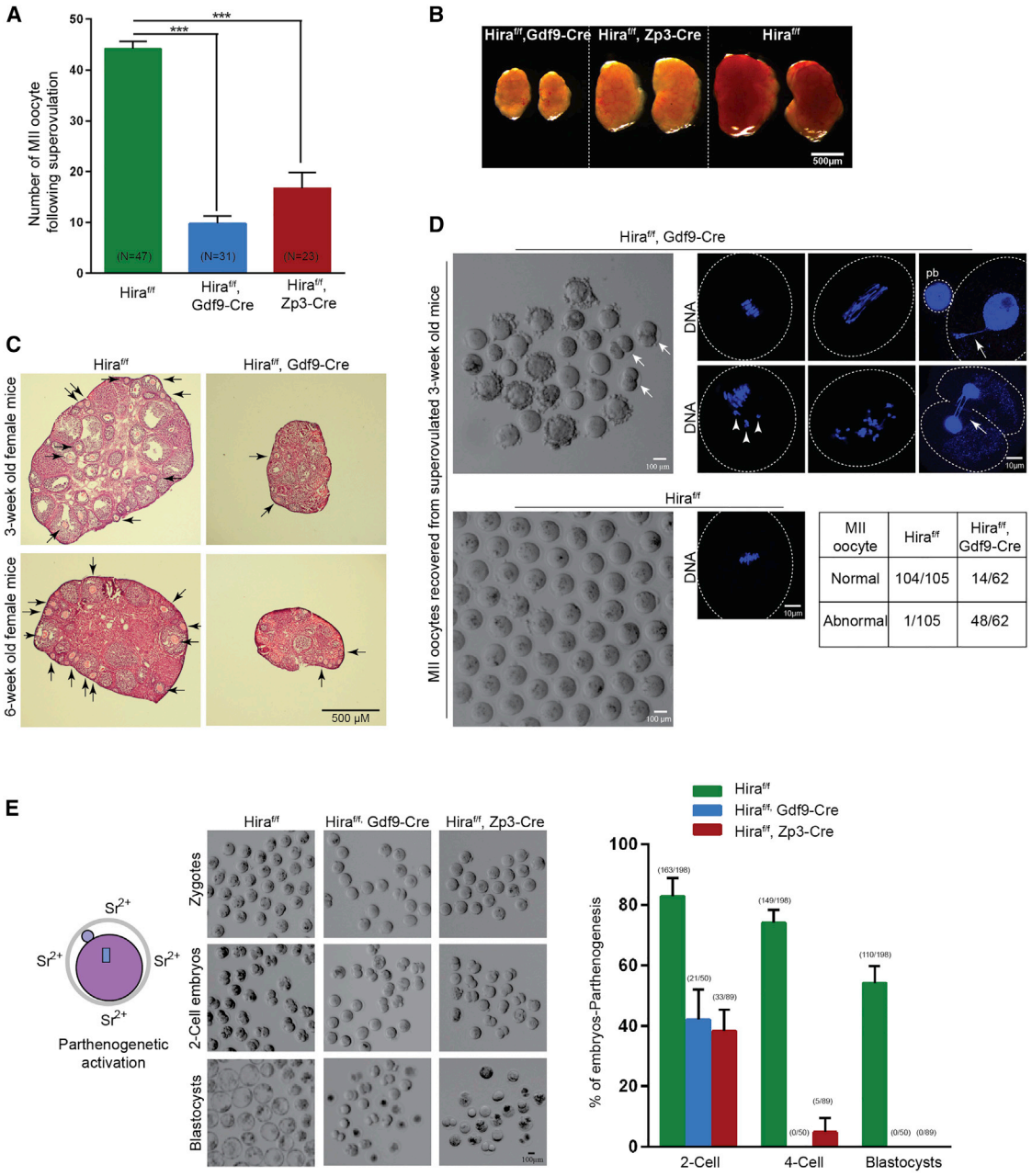

Figure 2. Hira Is Essential for Progression through Oogenesis and Acquisition of Developmental Competence

(A) Number of ovulated oocytes recovered per female after hormonal stimulation. Numbers of females scored are indicated in the columns. Error bars indicate SEM. ***$p < 0.001$; statistical analysis was carried out using two-tailed unpaired Student's t test.

(B) Ovaries of *Hira*$^{f/f}$, *Hira*$^{f/f}$ *Gdf9-Cre*$^{+}$, and *Hira*$^{f/f}$ *Zp3-Cre*$^{+}$ females were collected from mice born on the same date and ovarian images were taken in a single picture.

(C) Representative images show H&E staining of 3-week (top) and 6-week (bottom) ovarian sections (follicles indicated by arrows).

(D) Maternal Hira depletion results in defects in chromosome condensation and segregation. Representative bright-field images of MII oocytes recovered from two *Hira*$^{f/f}$ and two *Hira*$^{f/f}$ *Gdf9-Cre*$^{+}$ mice at 3 weeks of age are shown. Arrows (left) indicate oocytes with defective asymmetric division normally associated with first polar body extrusion (left). The oocytes were fixed and stained with DAPI (right). Arrows and arrowheads (right) indicate chromosome bridges and lagging chromosomes, respectively. Quantification of normal and abnormal MII oocytes is shown (bottom right).

(E) Early developmental arrest of parthenogenetic embryos with maternal Hira depletion. Representative images show embryos (left); quantification of developmental progression is shown (right). Oocytes lacking Hira do not progress beyond the two-cell stage. Embryo numbers are indicated above each column. Error bars indicate SEM. See also Figures S2, S3, and S4.

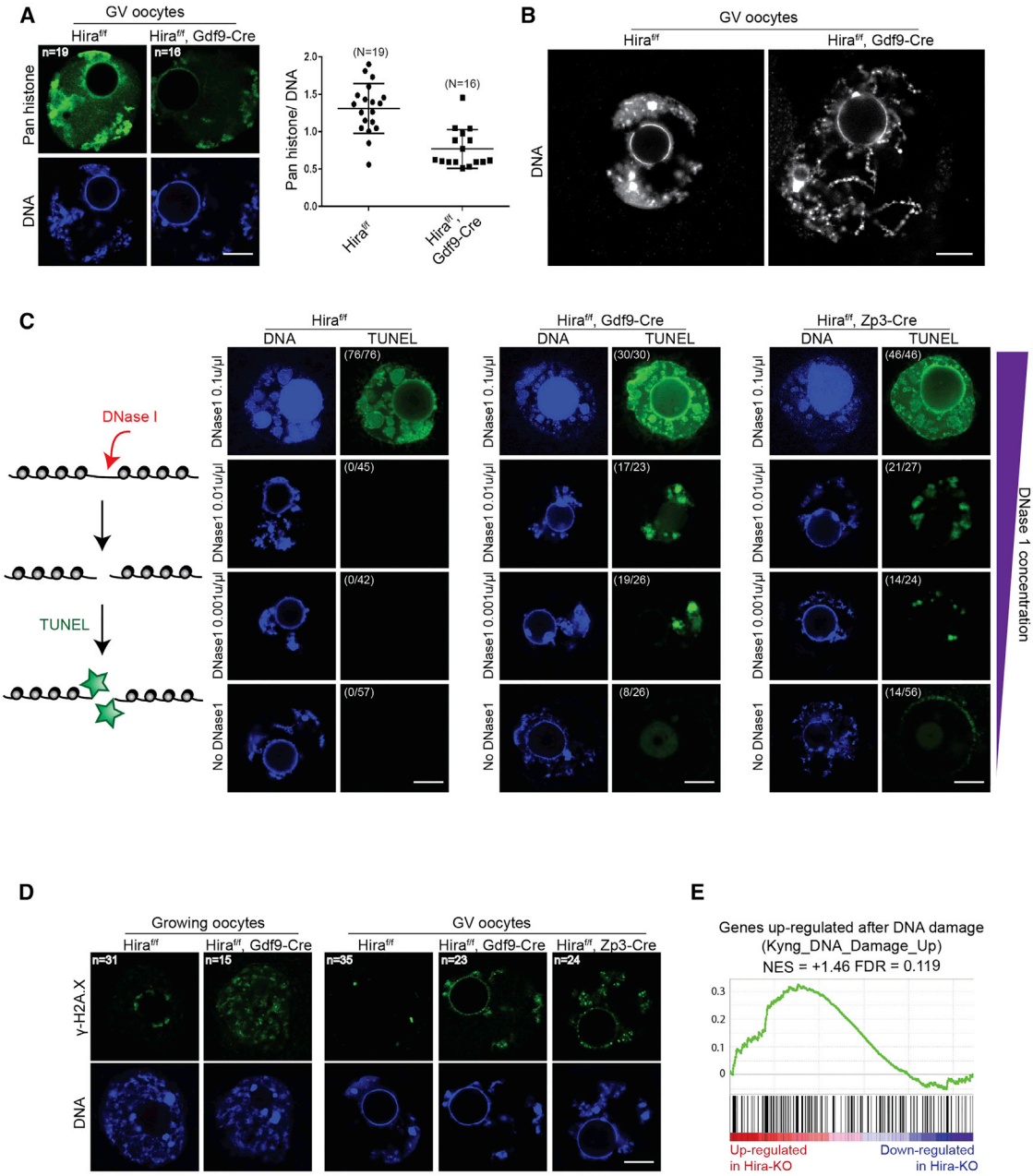

Figure 3. Hira Deletion Leads to Increased DNA Accessibility and Accumulation of DNA Damage

(A) Hira deletion leads to reduced histone load in the *Hira*$^{f/f}$ *Gdf9-Cre*$^{+}$ GV oocytes. The graph shows the quantification of the IF (pan histone antibody staining) signal normalized to DNA content (DAPI).

(B) Structural alteration of chromatin in *Hira*$^{f/f}$ *Gdf9-Cre*$^{+}$ GV oocytes. Extensive chromatin de-condensation was observed in more than half of the examined *Hira*$^{f/f}$ *Gdf9-Cre*$^{+}$ GV oocytes. DNA was stained with DAPI and pseudocolored in gray.

(C) Lack of Hira leads to increased DNase I accessibility. Schematic illustration shows in vivo DNase I TUNEL assay (left); see also the Supplemental Experimental Procedures. The fraction of oocytes with positive TUNEL signal is indicated in brackets.

(D) Lack of Hira leads to the accumulation of DNA damage. The γ-H2A.X staining of growing oocytes (P16, left) and GV oocytes (right) is shown.

(E) Gene set enrichment analysis (GSEA) compares genes upregulated after DNA damage (Kyng_DNA_Damage_Up gene set) and the ranked list of gene expression changes in *Hira*$^{f/f}$ *Gdf9-Cre*$^{+}$ relative to *Hira*$^{f/f}$ MII oocytes. NES, normalized enrichment score; FDR, false discovery rate (both were calculated in the GSEA program). DNA was stained with DAPI (in blue). Scale bar, 10 μm.

In agreement with the observed severe developmental phenotype, the initial data analysis revealed pronounced transcriptional differences upon deletion of *Hira* (Figures 4C and S6A). Expression analysis identified 2,101 differentially expressed genes (false discovery rate [FDR] < 0.1) between *Hira*$^{f/f}$ *Gdf9-Cre*$^{+}$ and control oocytes (1,274 upregulated in *Hira*$^{f/f}$ *Gdf9-Cre*$^{+}$ oocytes relative

to controls; 827 downregulated), representing over 15% of all annotated transcripts detected (Table S1). Gene ontology (GO) analysis of differentially upregulated genes showed enrichment for cell membrane, biological adhesion molecules, and cell junctions (Figure 4D). In contrast, GO analysis on differentially downregulated genes confirmed enrichment for processes important in late-stage oocytes, including chromosome, nucleolus, mitochondria, and pronucleus (Figure 4E).

Surprisingly, we detected significantly more annotated transcripts (7.7% increase, p value < 0.01) in *Hira*$^{f/f}$ *Gdf9-Cre*$^{+}$ oocytes relative to controls (Figure 4F). The increased number of transcripts was not evenly distributed across all expression levels (Figure 4G); rather, deletion of Hira resulted in relatively fewer transcripts with very low (first decile) or very high (ninth and tenth deciles) expression (Figure 4G). Furthermore, differentially down- and upregulated genes showed higher and lower than expected expression, respectively (Figure 4H); and, while the genes normally not expressed or expressed at very low levels (bottom 20%) were upregulated upon *Hira* deletion (Figure 4I; gene set enrichment analysis [GSEA], FDR < 0.001; data not shown), genes with very high expression in normal oocytes (top 20%) were specifically downregulated in *Hira*$^{f/f}$ *Gdf9-Cre*$^{+}$ oocytes (Figure 4I; GSEA, FDR < 0.001; data not shown). This also was evident by the greatly reduced variance in expression levels of annotated transcripts within the Hira-depleted oocytes (Figure 4J; p value < 0.001), suggesting that Hira is necessary to maintain the full dynamic range of gene expression. Thus, contrary to previous findings in proliferating pluripotent ESCs, Hira appears to be critical for normal transcriptional regulation during oocyte development.

The major transcriptional transition during oogenesis occurs between primordial stage oocytes (when *Gdf9*-driven Cre is first expressed) and primary stage oocytes (when *Zp3*-driven Cre is first expressed), during which the major wave of gene activation is observed (Pan et al., 2005). To test whether the observed transcriptional defects are due to *Hira*$^{f/f}$ *Gdf9-Cre*$^{+}$ oocytes failing to execute this transcriptional activation or to other dominant secondary effects, we additionally carried out scRNA-seq on four *Hira*$^{f/f}$ *Zp3-Cre*$^{+}$ and three *Hira*$^{f/f}$ control oocytes (Figure S6; Table S3). Remarkably, a nearly identical transcriptional phenotype was observed in *Hira*$^{f/f}$ *Zp3-Cre*$^{+}$ and *Hira*$^{f/f}$ *Gdf9-Cre*$^{+}$ oocytes: differentially down- and upregulated genes showed higher and lower than average expression in the control oocytes, respectively (Figure S6E), and genes normally not expressed or expressed at very low levels (bottom 20%) were upregulated upon Hira deletion (Figure S6F), while genes with very high expression in normal oocytes (top 20%) were specifically downregulated in *Hira*$^{f/f}$ *Gdf9-Cre*$^{+}$ oocytes (Figure S6F). Similar to the effect observed in *Hira*$^{f/f}$ *Gdf9-Cre*$^{+}$ oocytes, the variance in expression levels of annotated transcripts within the *Hira*$^{f/f}$ *Zp3-Cre*$^{+}$ oocytes was greatly reduced (Figure S6G; p value < 0.001).

Hira-Mediated H3.3/H4 Deposition Is Essential for Transcriptional Transitions Associated with the Oocyte Developmental Program

The developing oocyte is a unique experimental system, as it allows us to assess the importance of continuing histone H3.3/H4 replacement not only for steady-state transcription, but also for affecting transcriptional transitions associated with development, such as activation or repression of dynamically regulated genes. To address this, we used K-means clustering of published expression data (Pan et al., 2005; GEO: GSE3351) to identify eight clusters of genes that show distinct expression patterns over the course of oocyte development (Figures S5A and S5B), and we compared these to the expression profiles in *Hira*$^{f/f}$ *Gdf9-Cre*$^{+}$ and control oocytes. Remarkably, genes downregulated upon Hira depletion (*Hira*$^{f/f}$ *Gdf9-Cre*$^{+}$) were specifically enriched for genes whose transcription is activated either between the earliest stages of oocyte development (Figure 5A, cluster 4, primordial and primary follicle stages; GSEA, FDR < 0.001) or between early and late oogenesis (Figure 5A, cluster 5; GSEA, FDR < 0.001). In contrast, genes upregulated upon Hira deletion were most significantly enriched for clusters of genes that all uniquely show downregulation of expression between early and late oogenesis (Figure 5A, cluster 2; FDR = 0.017) or between primordial and primary follicle stages (Figure S5B, clusters 6 and 8). Of note, similar phenotypes were observed upon *Zp3*-Cre-driven deletion of Hira (Figure S6H).

To confirm that these observations were not an artifact of the reduced dynamic range observed in the Hira-depleted MII oocytes, we carried out a similar GSEA analysis on only median expressed genes (i.e., genes in the second, third, or fourth expression quintile). Cluster 2 (genes progressively downregulated during oogenesis) remained enriched among upregulated genes in *Hira*$^{f/f}$ *Gdf9-Cre*$^{+}$ oocytes (GSEA, FDR = 0.08; data not shown); similarly, cluster 4 (genes upregulated in early oogenesis) still showed enrichment (although this was less pronounced) among genes downregulated in the absence of Hira (GSEA, FDR = 0.26; data not shown). To further test the direct link between normal transcriptional activation and Hira, we carried out differential expression analysis between *Hira*$^{f/f}$ *Gdf9-Cre*$^{+}$ and *Hira*$^{f/f}$ *Zp3-Cre*$^{+}$ MII oocytes. Given the same observed reduction of the dynamic range of transcription in both systems (Figures 4G, 4J, and S6G), we hypothesized that, if normal transcriptional activation was dependent on Hira, genes that are specifically upregulated between primordial (when *Gdf9*-driven Cre is first expressed) and primary (when *Zp3*-driven Cre is first expressed) stage oocytes should show higher expression in *Hira*$^{f/f}$ *Zp3-Cre*$^{+}$ MII oocytes. Indeed, this hypothesis was confirmed by the GSEA analysis (Figure S6I; GSEA, FDR < 0.001).

Taken together, our data bring to light the critical role of Hira (and H3.3/H4 turnover) for affecting changes to the transcriptional state. Histone H3.3/H4 replacement is required for normal transcriptional activation of genes associated with developmental progression of oocytes, and, surprisingly, it is also necessary for genes to become or to remain transcriptionally silent.

Hira Depletion Leads to Aberrant Transcription from Regions Not Normally Transcribed within the Genome

Nucleosomes have been hypothesized to constitute a barrier for transcription (Teves et al., 2014). Considering the failure of Hira-deleted oocytes to silence genes, we asked whether the increased DNA accessibility in the absence of continuous H3.3/H4 replacement may lead to aberrant transcription from regions not normally transcribed within the genome. To address this possibility, we used a previously described approach that allows for the identification of unannotated transcripts originating entirely

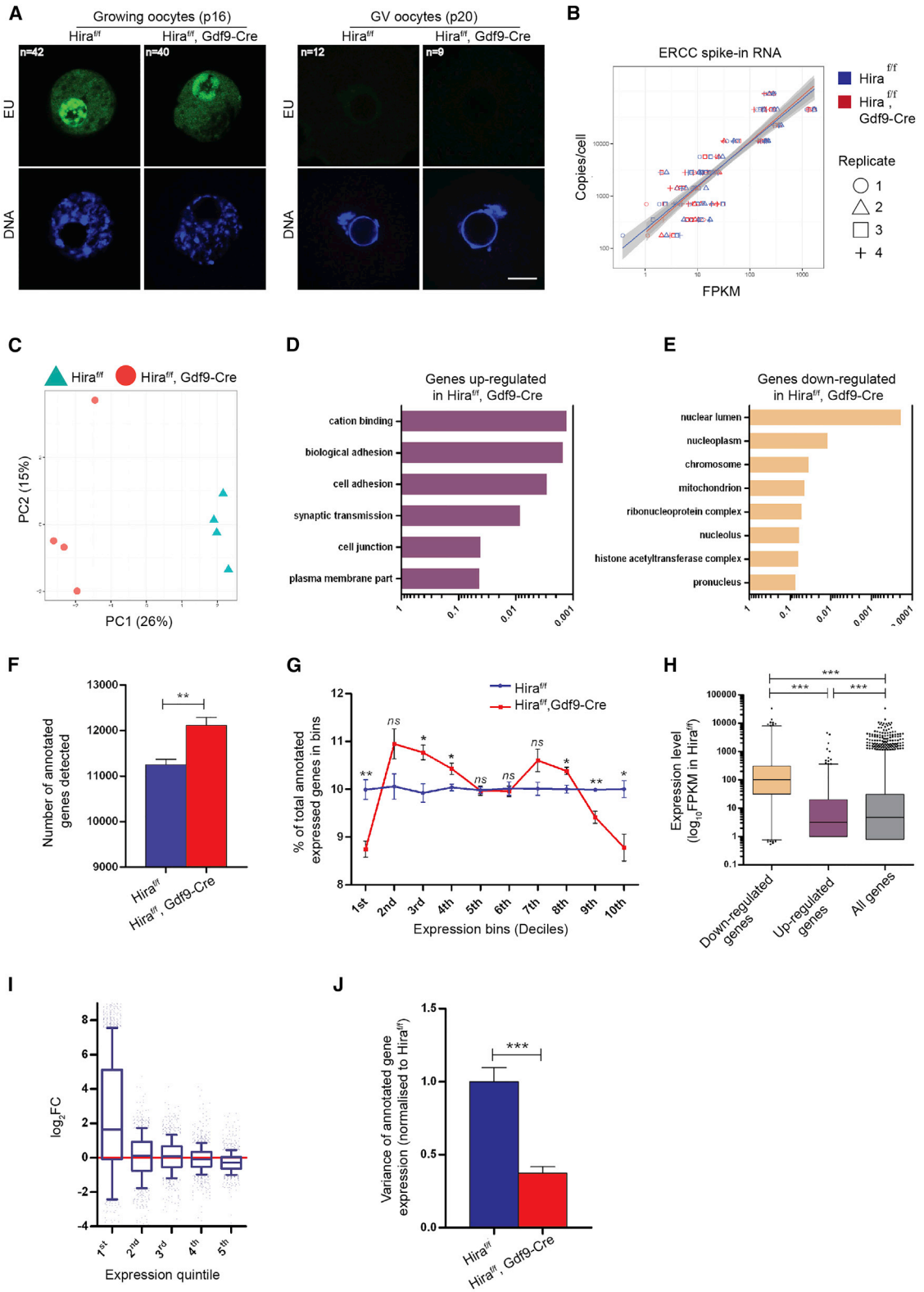

(legend on next page)

from intronic or intergenic regions (Trapnell et al., 2010). Consistent with our previous mapping, we observed an increase (7.3%, p value < 0.05) in the number of annotated transcripts detected in *Hira*$^{f/f}$ *Gdf9-Cre*$^{+}$ oocytes (Figure 5B). Remarkably, a much larger increase was observed in the total number of transcribed fragments (37.7%, p value < 0.05; Figure 5B), with the largest increases observed in unannotated transcripts originating entirely from intronic (112.6% increase, p value < 0.05) and intergenic (92.0% increase, p value < 0.05) regions (Figure 5C) of the *Hira*-deleted oocytes. Of note, while expression of unannotated intergenic transcripts was clearly detectable (90% transcripts with >1 fragments per kilobase of transcript per million mapped reads [FPKM]) and often at high level (8% transcripts with >10 FPKM) in individual knockout samples, expression of a given unannotated intergenic transcript was only ever observed in one biological replicate, reflecting stochastic events consistent with spurious transcription (Table S2). Also of note, a nearly identical phenotype was observed upon *Zp3*-Cre-driven deletion of *Hira* (Figures S6D, S6J, and S6K; Table S4).

Continuing Histone Replacement Is Essential for Efficient De Novo Methylation during Oogenesis

Progression through oocyte development is accompanied by the accumulation of DNA methylation. During this process, the largely hypomethylated genome of primordial oocytes acquires DNA methylation through the activity of the de novo DNA methyltransferase Dnmt3a and its co-factor Dnmt3l (Kaneda et al., 2004; Smallwood and Kelsey, 2012; Smallwood et al., 2011). Acquisition of DNA methylation in oocytes is known to be positively correlated with transcription, which could relate to the recruitment of Dnmt3a/3l to gene bodies through binding of its PWWP domain to H3K36me3, a histone modification associated with transcriptional elongation (Chotalia et al., 2009; Dhayalan et al., 2010; Kobayashi et al., 2012; Veselovska et al., 2015). Although H3K36me3-driven DNA methylation in gene bodies has recently been attributed to the enzymatic activity of Dnmt3b in mouse ESCs (Baubec et al., 2015; Yang et al., 2014), Dnmt3a is responsible for the accumulation of oocyte DNA methylation as Dnmt3b is absent in growing oocytes (Kaneda et al., 2004; Shirane et al., 2013). Given the widespread transcriptional changes observed in the Hira knockout oocytes, we set out to examine the potential impact of Hira deletion on de novo DNA methylation in the oocyte.

Although the total amount of transcription was not altered upon *Hira* deletion (Figures 4A and 4B), the observed reduced histone load was connected with lower levels of global H3K36me3 in Hira-depleted GV oocytes (Figures 3A and S7A). Interestingly, initial immunofluorescence (IF) detection of 5mC indicated that *Hira*$^{f/f}$ *Gdf9-Cre*$^{+}$ GV oocytes also contain lower levels of DNA methylation (Figure S7B). Further quantitative assessment by liquid chromatography-mass spectrometry (LC-MS) revealed a dramatic reduction of 5mC in *Hira*-deleted oocytes, with a more pronounced effect following earlier *Gdf9-Cre*$^{+}$-driven deletion (Figure 6A). Importantly, the reduction of DNA methylation occurred despite the transcriptional upregulation of *Dnmt3a* and without statistically significant changes in the expression of other DNA methyltransferases (Figures S5C, S7C, and S7D).

To further understand the relationship among Hira deletion, transcriptional changes, and global changes in DNA methylation, we profiled DNA methylation genome-wide by bisulphite sequencing. Because of the very limited availability of *Hira*-deleted oocytes, we performed single-cell bisulphite sequencing (scBS-seq) on 14 individual *Hira*$^{f/f}$ *Gdf9-Cre*$^{+}$ MII oocytes and 14 individual *Hira*$^{f/f}$ control MII oocytes, followed by in silico merging of the individual datasets, as previously described (Smallwood et al., 2014). We first confirmed that our scBS-seq dataset represented an accurate depiction of oocyte methylation, as we observed a high correlation (R = 0.96) between our merged scBS-seq control oocytes and an independent whole-genome bisulphite sequencing (WGBS) dataset of pooled oocytes (Shirane et al., 2013; DNA Data Bank of Japan: DRA000570; Figures 6C and S7E). In agreement with the LC-MS measurements and IF data, our WGBS analysis confirmed the dramatic reduction in DNA methylation in both CpG (42.7% decrease) and CHH (73.2% decrease) contexts (Figures 6B and S7F). Further analysis revealed that only 3.8% of the 3-kb genomic windows classed as methylated in wild-type oocytes (>80% methylation) remained methylated to the same extent in Hira-depleted oocytes, with the majority of methylated (>80%) regions showing less than 50% DNA methylation in Hira-depleted oocytes (Figure 6D). At the whole-genome level, 40.2% of 3-kb genomic windows displayed a statistically significant loss of DNA methylation in *Hira*$^{f/f}$

Figure 4. Continuous Histone Replacement Mediated by Hira Is Required to Maintain the Full Dynamic Range of Gene Expression

(A) Detection of newly synthesized RNA by EU incorporation in growing (P14) and GV (P20) *Hira*$^{f/f}$ and *Hira*$^{f/f}$ *Gdf9-Cre*$^{+}$ oocytes is shown. Scale bar, 10 μm.

(B) Comparison between obtained FPKM values and absolute copy number per cell for ERCC spike-in RNA in *Hira*$^{f/f}$ and *Hira*$^{f/f}$ *Gdf9-Cre*$^{+}$ MII oocytes revealed no significant difference.

(C) Principal component analysis of scRNA-seq data derived from *Hira*$^{f/f}$ and *Hira*$^{f/f}$ *Gdf9-Cre*$^{+}$ MII oocytes is shown.

(D and E) Selected gene ontology (GO) terms significantly enriched for among differentially upregulated (D, edgeR, FDR < 0.1) and differentially downregulated (E, edgeR, FDR < 0.1) genes in *Hira*$^{f/f}$ *Gdf9-Cre*$^{+}$ MII oocytes are shown. x axis represents Benjamini-Hochberg adjusted p value.

(F) Number of annotated genes detected, as computed by HTSeq program, is shown.

(G) Relative proportion of genes distributed among ten equally sized expression level bins. All genes detected in our RNA-seq experiment were divided into ten equal bins based on their expression levels in *Hira*$^{f/f}$ oocytes. The gene number in each bin was counted for *Hira*$^{f/f}$ or *Hira*$^{f/f}$ *Gdf9-Cre*$^{+}$, and the percentage was calculated relative to all genes detected in a given sample.

(H) Boxplot shows gene expression levels of differentially upregulated (edgeR, FDR < 0.1), downregulated (edgeR, FDR < 0.1), and all annotated genes in *Hira*$^{f/f}$ *Gdf9-Cre*$^{+}$ MII oocytes.

(I) Boxplots show distribution of gene expression fold change for each gene expression level quintile (based on *Hira*$^{f/f}$ gene expression levels).

(J) Variance of gene expression within a given *Hira*$^{f/f}$ or *Hira*$^{f/f}$ *Gdf9-Cre*$^{+}$ sample. In all cases, error bars indicate SEM. Statistical analysis was carried out using two-tailed unpaired Student's t test (F and G), Kruskal-Wallis with Dunn's post hoc test (H) or F test (J); ns, non-significant; *p < 0.05, **p < 0.01, and ***p < 0.001. See also Figure S6.

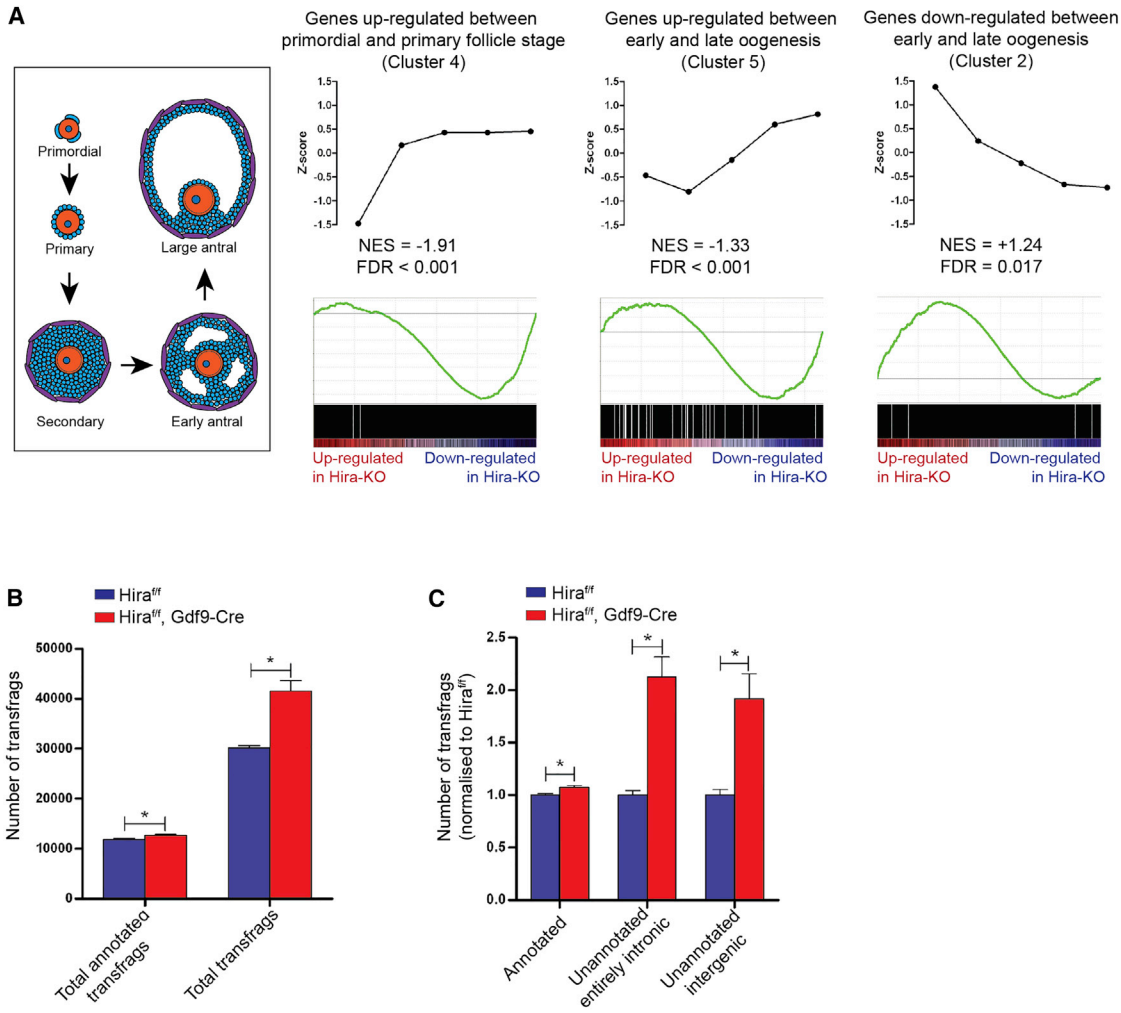

Figure 5. Hira Is Essential for Transcriptional Transitions Associated with the Oocyte Developmental Program and Is Required for Repression of Aberrant Transcription

(A) GSEA comparing genes of selected expression clusters during oogenesis (Figure S5B) and the ranked list of gene expression changes in *Hira*$^{f/f}$ *Gdf9-Cre*$^{+}$ MII oocytes relative to *Hira*$^{f/f}$ oocytes. NES and FDR both were calculated in the GSEA program. For each cluster, each dot represents mean-normalized gene expression for consecutive stages of oocyte development.

(B) Numbers of total transfrags and total annotated transfrags in *Hira*$^{f/f}$ and *Hira*$^{f/f}$ *Gdf9-Cre*$^{+}$ MII oocytes (as computed by CuffCompare program) are shown.

(C) Numbers of total annotated transfrags, unannotated entirely intronic transfrags, and unannotated entirely intergenic transfrags in *Hira*$^{f/f}$ and *Hira*$^{f/f}$ *Gdf9-Cre*$^{+}$ MII oocytes (as computed by CuffCompare program) are shown. In all cases, error bars indicate SEM. Statistical analysis was carried out using two-tailed Student's t test (*$p < 0.05$). See also Figures S5 and S6.

Gdf9-Cre^{+} oocytes (Figure 6E; chi-square test, $p < 0.001$). This extensive reduction of DNA methylation was observed across all types of genomic regions, including genic regions, CpG islands, maternally methylated imprint control regions, and repetitive elements (Figures 6F, 6G, S7G, and S7H).

In agreement with previously published observations (Kobayashi et al., 2012; Veselovska et al., 2015), we observed a positive correlation between transcription and the level of DNA methylation in control oocytes (Figure 6H). Although the methylome of *Hira*$^{f/f}$ *Gdf9-Cre*$^{+}$ oocytes was severely reduced in comparison to control oocytes, they too retained a positive correlation between transcription and DNA methylation across most of the transcriptional range (Figure 6H); however, this correlation was abolished for highly expressed genes (Figure 6H). Consequently, the effect on DNA methylation in *Hira*-deleted oocytes was more pronounced at highly expressed genes compared to median expressed genes (Figure S7I). Surprisingly, beyond the observed relationship between transcription level and DNA methylation described above, on average, DNA methylation was reduced both at genes whose expression was unaffected by *Hira* deletion and also at genes differentially expressed between control and *Hira*$^{f/f}$ *Gdf9-Cre*$^{+}$ oocytes, regardless of whether they were up- or downregulated (Figure 6I). Cumulatively, these observations suggest that, although de novo methylation is still targeted to transcribed regions in Hira-depleted oocytes, this process appears to be inefficient, clearly indicating that transcription is

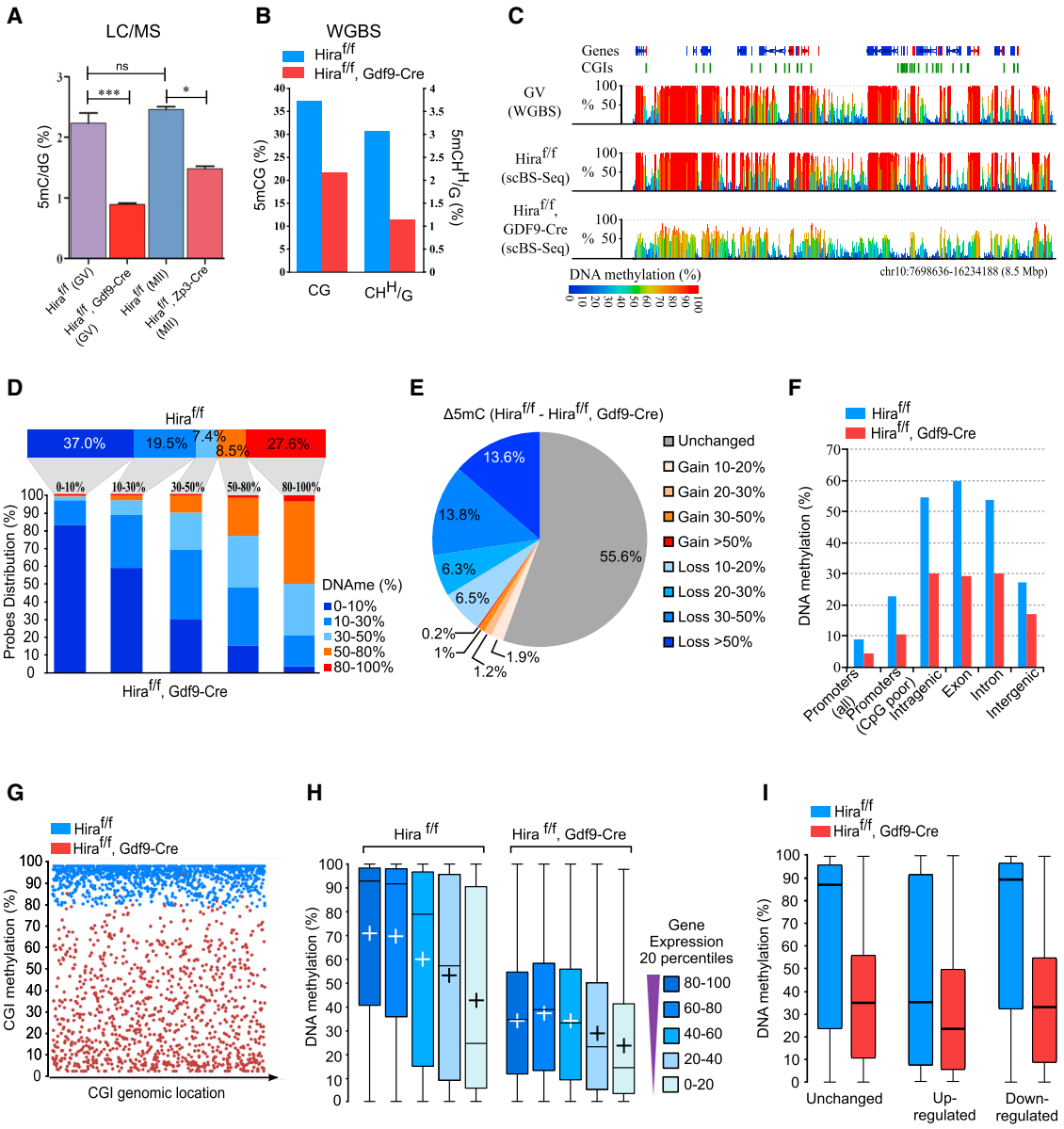

Figure 6. Continuous Histone Replacement Is Required for Efficient De Novo Methylation during Oogenesis

(A) Reduced total 5mC was measured by LC-MS in GV (*Hira*$^{f/f}$ and *Hira*$^{f/f}$ *Gdf9-Cre*$^{+}$) and MII (*Hira*$^{f/f}$ and *Hira*$^{f/f}$ *Zp3-Cre*$^{+}$) oocytes.

(B) Global levels of DNA methylation quantified by scBS-seq in the CpG (CG) and non-CpG (CHH/G) contexts are shown.

(C) Example shows CpG methylation quantified over 3-kb sliding windows (1.5-kb steps) for published GV datasets (Shirane et al., 2013; WGBS, top), *Hira*$^{f/f}$, and *Hira*$^{f/f}$ *Gdf9-Cre*$^{+}$ (scBS-seq).

(D) Distribution shows the 3-kb genomic windows in the indicated bins of DNA methylation in *Hira*$^{f/f}$ oocytes (top, horizontal, percentage indicating the proportion of methylation bins) and their corresponding DNA methylation values in *Hira*$^{f/f}$ *Gdf9-Cre*$^{+}$ oocytes (bottom, vertical columns).

(E) Pie chart distribution shows the 3-kb genomic windows presenting statistically significant (chi-square test, $p < 0.01$) changes in *Hira*$^{f/f}$ *Gdf9-Cre*$^{+}$ versus *Hira*$^{f/f}$ (percentage indicates the proportion of each segment).

(F) Effect of Hira deletion on DNA methylation is global and independent of the genomic context. DNA methylation at CpGs (five reads coverage) was determined and averaged for each genomic context.

(G) CpG islands (CGIs) methylated in *Hira*$^{f/f}$ oocytes are globally hypomethylated in *Hira*$^{f/f}$ *Gdf9-Cre*$^{+}$ oocytes. CGI methylation was defined for each genotype, and only CGIs hypermethylated in *Hira*$^{f/f}$ (>80%) are displayed, for both *Hira*$^{f/f}$ (blue) and *Hira*$^{f/f}$ *Gdf9-Cre*$^{+}$ (red), and ordered on the x axis based on their genomic location.

(H) Effects on DNA methylation in *Hira*$^{f/f}$ *Gdf9-Cre*$^{+}$ oocytes are more pronounced at highly expressed genes. DNA methylation was quantified for genes binned into expression percentile based on the scRNA-seq data (boxplot with plus signs representing mean values and horizontal bars representing median values).

(I) Comparison between DNA methylation and gene expression differences in *Hira*$^{f/f}$ and *Hira*$^{f/f}$ *Gdf9-Cre*$^{+}$ oocytes. See also Figure S7.

not sufficient to ensure normal levels of de novo DNA methylation in this system.

Considering the high levels of Dnmt3a and Dnmt3l in *Hira*$^{f/f}$ *Gdf9-Cre*$^{+}$ oocytes (Figures S7C and S7D), we reasoned that the observed effect was likely caused either by inefficient recruitment or reduced enzymatic activity on chromatin of the Dnmt3a/3l complex. We first asked whether chromatin association of Dnmt3a is grossly altered following Hira depletion in *Hira*$^{f/f}$ *Gdf9-Cre*$^{+}$ oocytes. In agreement with our RNA-seq and qPCR data, Hira knockout oocytes contained higher levels of Dnmt3a (Figures S7C, S7D, and S5C). Importantly, Dnmt3a remained associated with chromatin following Triton pre-extraction of soluble proteins, confirming that altered chromatin structure in *Hira*-deleted oocytes does not completely abolish recruitment of this enzyme (Figure S7J).

In this context, the PWWP domain of Dnmt3a has previously been shown to interact in vitro with H3K36me3 (Dhayalan et al., 2010). Although the recognition of this histone modification by Dnmt3b (and not by Dnmt3a) has recently been linked to gene body DNA methylation in mouse ESCs (Baubec et al., 2015), it is possible that reduced H3K36me3 levels observed in Hira-depleted GV oocytes contribute to the observed loss of DNA methylation in this system. In addition, using in vitro biochemical assays, it has recently been shown that the enzymatic activity of Dnmt3a is specifically enhanced by binding to the N-terminal tail of histone H3 lacking methylation at lysine 4 (H3K4me0) (Guo et al., 2015). Despite the lack of H3.3/H4 replacement, growing *Hira*$^{f/f}$ *Gdf9-Cre*$^{+}$ oocytes remained highly transcriptionally active (Figure 4A). It is, thus, conceivable that passage of the transcriptional machinery would result in histone H3 depletion and increased DNA accessibility, both of which we observed (Figures 3A and 3C). Although our developmental system precludes direct analysis of locus-specific histone turnover due to severely limited material, a very strong correlation had been observed previously between transcription levels and the degree of histone (and specifically H3.3) replacement, a relationship that is conserved among various model organisms including mouse (Deal et al., 2010; Kraushaar et al., 2013; Mito et al., 2005; Wirbelauer et al., 2005). In agreement with this, DNA methylation was most affected at genes with the highest level of transcription (Figures 6H and S7I). We also note that, while the combination of both compromised Dnmt3a/3l recruitment and reduced enzymatic activity would explain the reduction of DNA methylation in transcribed regions, reduced histone load is likely to underpin the methylation defect observed in other non-transcribed parts of the genome (Figure 6F; Guo et al., 2015).

DISCUSSION

To address the biological significance of continuous histone replacement in a physiological context, we have generated a genetic deletion of the histone chaperone *Hira* in the early stages of mouse oogenesis. Developing mouse oocytes represent a unique experimental system as postnatal oocytes undergo developmental transitions, including major transcriptional changes and widespread de novo DNA methylation, in the absence of DNA replication. Our results show that the chromatin of developing oocytes is highly dynamic, with histone turnover being observed also in the transcriptionally inert GV-stage oocytes (Figures 1C and 4A). We demonstrate that constant histone replacement is necessary for the maintenance of normal chromatin homeostasis in vivo. Depletion of Hira during early oocyte development leads to a severe reduction of histone load, compromised developmental progression, and progressive oocyte loss (Figures 2, 3A, and S2G). We note that, albeit pronounced, our observed phenotype is milder in comparison to the recently reported oocyte death in H3.3 knockout mice (Tang et al., 2015). We attribute this difference to the presence of an alternative ATRX/DAXX H3.3 chaperone complex, which, although present in our system, cannot functionally replace Hira-driven H3.3 deposition (Figures S2A–S2C).

Our experiments document that, while lacking the normal ability to incorporate H3.3 and H4, *Hira*-deleted growing oocytes remain transcriptionally active, which results in chromatin with severely reduced histone content, increased DNase I sensitivity, and signs of DNA damage (Figures 3 and S2B). Reminiscent of the phenotype associated with Hira depletion in yeast (Blackwell et al., 2004; Greenall et al., 2006) and H3.3 depletion in mice (Bush et al., 2013; Lin et al., 2013) and *Drosophila* (Sakai et al., 2009), the compromised chromatin structure leads to chromosome segregation defects and aberrant first polar body extrusion (Figure 2D). However, the observed chromosome segregation defects in the Hira-depleted oocytes are not linked with aberrant CenpA incorporation, as previously suggested in somatic cells (Figure S2C; Bush et al., 2013).

Non-replicative Hira-depleted oocytes uniquely reveal the importance of histone replacement on transcriptional regulation in the absence of replication-coupled chromatin assembly. Although transcription can continue from histone-depleted chromatin, our study shows that the lack of histone replacement has a major impact on the dynamic range of gene expression. In the context of histone-depleted chromatin, genes can neither be efficiently silenced nor effectively activated. Additionally, the lack of normal histone occupancy leads to increased spurious transcription from otherwise not-transcribed regions of the genome, suggesting an evolutionarily conserved role for the Hira histone chaperone complex (Anderson et al., 2009).

Our results additionally reveal an unexpected connection among continuous H3.3 replacement, transcription, and de novo DNA methylation in developing oocytes. Following Hira depletion, more accessible chromatin with reduced histone load leads to significantly reduced DNA methylation (Figures 6A–6G). We note that, although in other systems DNA methylation changes result in pronounced transcriptional outcomes (Yang et al., 2014), reduced DNA methylation is not likely to contribute to the observed transcriptional changes in Hira-depleted oocytes, as *Dnmt3l* knockout oocytes lacking DNA methylation do not display any transcriptional phenotype (Kobayashi et al., 2012).

Our data suggest that the observed methylation phenotype cannot be attributed to downregulation of the Dnmt3a/3l complex, and, although we cannot exclude locus-specific effects on Dnmt3a/3l recruitment, the observed reduced DNA methylation is likely due to altered enzymatic activity of Dnmt3a in the absence of normal levels of chromatin-bound H3 (Figures 1C, 1E, and S2B). In this context, the N-terminal part of H3 has

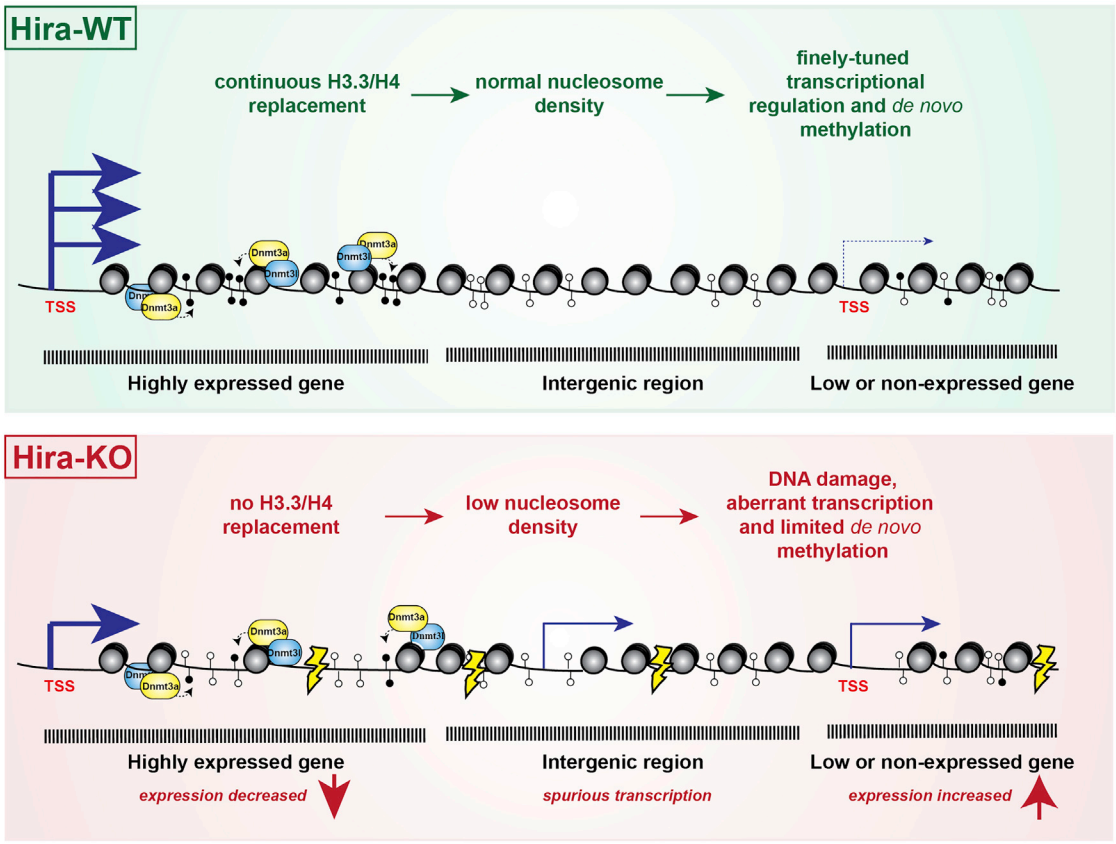

Figure 7. Role of Hira in Transcriptional Regulation and De Novo DNA Methylation during Oogenesis

During oogenesis, normal chromatin structure and nucleosome density is maintained by Hira-mediated continuous H3.3/H4 replacement. This is required for fine-tuned transcriptional regulation and efficient de novo DNA methylation.

been shown in vitro to be required for allosteric activation of Dnmt3a catalytic activity (Guo et al., 2015). Our study thus provides the first support for this effect in an in vivo setting. The observed effect is more pronounced in highly expressed genes (Figure S7I), in agreement with the expected role of transcription in inducing nucleosome depletion in Hira-depleted oocytes. Furthermore, CpG island methylation is greatly reduced in Hira-depleted oocytes (Figure 6G) and methylation loss is more pronounced at regions with high CpG density (Figure S7K). As the Dnmt3a enzyme has been shown to operate in a non-processive manner (Dhayalan et al., 2010), stimulatory effect of the unmodified (H3K4me0) H3 tail might be necessary to ensure a high level of methylation at these regions.

We also considered that loss of Hira early during oocyte development (*Gdf9-Cre*-driven deletion) might lead to a variety of secondary effects that could contribute to the observed phenotypes. In this context it is important to note that deletion of *Hira* at a later time point during oogenesis (*Zp3-Cre* system) fully recapitulated the transcriptional and DNA methylation defects observed in *Hira*$^{f/f}$ *Gdf9-Cre*$^{+}$ oocytes (Figures 6A and S6), providing further support for our findings and indicating that the observed effects are not solely attributable to compromised development of the oocytes. Although we cannot exclude that some of the effects could be secondary to alterations in gene expression, the most parsimonious view is that the abnormal chromatin resulting from impaired H3.3/H4 deposition is responsible for the majority of the phenotypes we observed.

In addition, while it is important to consider that the observed transcriptional and methylation effects could be connected with the specific absence of the H3.3 variant upon Hira depletion in oocytes (Santenard et al., 2010), it is likely that the lack of normal chromatin structure due to the inability to continuously replace H3/H4 is the main cause underlying the described phenotype. Consistent with this view, the pronounced transcriptional phenotype observed in Hira-depleted oocytes is in stark contrast to the only limited transcriptional changes previously described in *Hira* knockout ESCs (Banaszynski et al., 2013; Goldberg et al., 2010). In that case, replication-dependent deposition of canonical H3 by the Caf1 complex was likely to compensate in the absence of Hira-mediated H3.3 deposition in rapidly dividing ESCs (Banaszynski et al., 2013; Goldberg et al., 2010). Indeed, H3.3 depletion does not lead to pronounced changes in nucleosome occupancy in proliferating ESCs (Banaszynski et al., 2013). In contrast, our findings document that post-replicative cells in vivo require continuous histone replacement in order to maintain an intact chromatin structure, which in turn is required for normal regulation of transcription and for de novo DNA methylation in

the context of developing oocytes (Figure 7). Interestingly, the critical role of continuous histone replacement also has been demonstrated recently in post-mitotic neurons, where the lack of H3.3 incorporation had an impact on both transcription and physiological function of neurons (Maze et al., 2015, published while our manuscript was under review). Collectively, our studies thus provide new insights into the histone dynamics in vivo and highlight the importance of studying chromatin in a physiological context and in non-proliferating post-mitotic cells.

EXPERIMENTAL PROCEDURES

Mice

Hira (*Hira*$^{f/f}$) mice were generated by the Wellcome Trust Sanger Institute. Oocyte-specific Hira depletion was achieved by crossing *Hira*$^{f/f}$ mice with *Gdf9-iCre* or with *Zp3-Cre* mice, respectively. The H3.3B-EGFP knockin strain was generated in the MRC CSC transgenic facility and protamine 1-EGFP strain was generated by Dr. P. Pelczar. All animal experiments were carried out under a UK Home Office Project License in a Home Office-designated facility. Detailed information is available in the Supplemental Experimental Procedures.

Oocyte/Embryo Culture, mRNA Microinjection, IF, and H&E Staining

In vitro fertilization (IVF), in vitro maturation (IVM), parthenogenesis, mRNA microinjection, TUNEL assay, IF, and H&E staining were carried out as described previously (Hajkova et al., 2010; Nashun et al., 2010). Detailed information is available in the Supplemental Experimental Procedures.

scRNA-Seq

The scRNA-seq was performed on *Hira*$^{f/f}$, *Hira*$^{f/f}$ *Gdf9-Cre*$^{+}$, and *Hira*$^{f/f}$ *Zp3-Cre*$^{+}$ MII oocytes using the SMARTer Ultra Low Input RNA kit (Clontech Laboratories) with ERCC RNA spike-in mix 1 (Life Technologies). Detailed information is available in the Supplemental Experimental Procedures.

DNA Methylation Analysis

An scBS-seq described previously (Smallwood et al., 2014) was used to profile the DNA methylation landscape of *Hira*$^{f/f}$ and *Hira*$^{f/f}$ *Gdf9-Cre*$^{+}$ oocytes. Ultra-sensitive LC-MS was used to determine overall 5-methylcytosine level. For detailed information, see the Supplemental Experimental Procedures.

ACCESSION NUMBERS

The accession numbers for the sequencing reported in this paper are GEO GSE66931, GSE73382, and GSE66629.

SUPPLEMENTAL INFORMATION

Supplemental Information includes Supplemental Experimental Procedures, seven figures, and four tables and can be found with this article online at http://dx.doi.org/10.1016/j.molcel.2015.10.010.

AUTHOR CONTRIBUTIONS

P.H. and B.N. conceived the study. B.N. performed the experiments and analyzed the data together with P.H. P.W.S.H. carried out scRNA-seq and analyzed the data with G.D. S.A.S. and S.J.C. carried out scBS-seq and S.A.S. analyzed the data with G.K. and P.W.S.H. R.A. carried out LC-MS experiments and analyzed the data. R.J.F. and V.S. provided original *Hira*$^{f/f}$ mice and *EGFP-H3.3* knockin vector. R.J.F. contributed to the data analysis and the interpretation of the experiments. E.N. conducted ESC targeting and generated *EGFP-H3.3* chimeras. P.P. re-derived and provided the Protamine1-EGFP mice for this study. P.H., B.N., and P.W.S.H. wrote the manuscript with assistance from S.A.S., G.K., and R.J.F. P.W.S.H. and S.A.S. contributed equally to this work.

ACKNOWLEDGMENTS

We are grateful to the members of the P.H. lab and to Naveenan Navaratnam for discussions and revision of the manuscript. We thank the MRC CSC microscopy facility (Dirk Dormann and Chad Whilding) for help with microscopy and imaging; Megan Woodberry, Emma Francis, Darran Hardy, and Justyna Glegola for mouse husbandry; and Heba Saadeh for bioinformatics support. We also thank the MRC transgenic facility (Zoe Webster) for help regarding microinjection. Work in the P.H. lab is supported by the MRC funding to P.H. (MC_US_A652_5PY70) and by FP7 EpiGeneSys network. G.K.'s lab is supported by grants from the MRC and Biotechnology and Biological Sciences Research Council (BBSRC). P.H. is a member of EMBO Young Investigator Programme. B.N. is a recipient of a Marie Curie International Incoming Fellowship (FP7).

Received: February 24, 2015
Revised: July 7, 2015
Accepted: October 2, 2015
Published: November 5, 2015

REFERENCES

Adam, S., Polo, S.E., and Almouzni, G. (2013). Transcription recovery after DNA damage requires chromatin priming by the H3.3 histone chaperone HIRA. Cell *155*, 94–106.

Akiyama, T., Suzuki, O., Matsuda, J., and Aoki, F. (2011). Dynamic replacement of histone H3 variants reprograms epigenetic marks in early mouse embryos. PLoS Genet. *7*, e1002279.

Anderson, H.E., Wardle, J., Korkut, S.V., Murton, H.E., López-Maury, L., Bähler, J., and Whitehall, S.K. (2009). The fission yeast HIRA histone chaperone is required for promoter silencing and the suppression of cryptic antisense transcripts. Mol. Cell. Biol. *29*, 5158–5167.

Banaszynski, L.A., Wen, D., Dewell, S., Whitcomb, S.J., Lin, M., Diaz, N., Elsässer, S.J., Chapgier, A., Goldberg, A.D., Canaani, E., et al. (2013). Hira-dependent histone H3.3 deposition facilitates PRC2 recruitment at developmental loci in ES cells. Cell *155*, 107–120.

Baubec, T., Colombo, D.F., Wirbelauer, C., Schmidt, J., Burger, L., Krebs, A.R., Akalin, A., and Schübeler, D. (2015). Genomic profiling of DNA methyltransferases reveals a role for DNMT3B in genic methylation. Nature *520*, 243–247.

Blackwell, C., Martin, K.A., Greenall, A., Pidoux, A., Allshire, R.C., and Whitehall, S.K. (2004). The Schizosaccharomyces pombe HIRA-like protein Hip1 is required for the periodic expression of histone genes and contributes to the function of complex centromeres. Mol. Cell. Biol. *24*, 4309–4320.

Burgess, R.J., and Zhang, Z. (2013). Histone chaperones in nucleosome assembly and human disease. Nat. Struct. Mol. Biol. *20*, 14–22.

Bush, K.M., Yuen, B.T., Barrilleaux, B.L., Riggs, J.W., O'Geen, H., Cotterman, R.F., and Knoepfler, P.S. (2013). Endogenous mammalian histone H3.3 exhibits chromatin-related functions during development. Epigenetics Chromatin *6*, 7.

Chotalia, M., Smallwood, S.A., Ruf, N., Dawson, C., Lucifero, D., Frontera, M., James, K., Dean, W., and Kelsey, G. (2009). Transcription is required for establishment of germline methylation marks at imprinted genes. Genes Dev. *23*, 105–117.

De La Fuente, R. (2006). Chromatin modifications in the germinal vesicle (GV) of mammalian oocytes. Dev. Biol. *292*, 1–12.

Deal, R.B., Henikoff, J.G., and Henikoff, S. (2010). Genome-wide kinetics of nucleosome turnover determined by metabolic labeling of histones. Science *328*, 1161–1164.

Dhayalan, A., Rajavelu, A., Rathert, P., Tamas, R., Jurkowska, R.Z., Ragozin, S., and Jeltsch, A. (2010). The Dnmt3a PWWP domain reads histone 3 lysine 36 trimethylation and guides DNA methylation. J. Biol. Chem. *285*, 26114–26120.

Goldberg, A.D., Banaszynski, L.A., Noh, K.M., Lewis, P.W., Elsaesser, S.J., Stadler, S., Dewell, S., Law, M., Guo, X., Li, X., et al. (2010). Distinct factors control histone variant H3.3 localization at specific genomic regions. Cell *140*, 678–691.

Greenall, A., Williams, E.S., Martin, K.A., Palmer, J.M., Gray, J., Liu, C., and Whitehall, S.K. (2006). Hip3 interacts with the HIRA proteins Hip1 and Slm9 and is required for transcriptional silencing and accurate chromosome segregation. J. Biol. Chem. *281*, 8732–8739.

Guo, X., Wang, L., Li, J., Ding, Z., Xiao, J., Yin, X., He, S., Shi, P., Dong, L., Li, G., et al. (2015). Structural insight into autoinhibition and histone H3-induced activation of DNMT3A. Nature *517*, 640–644.

Gurard-Levin, Z.A., Quivy, J.P., and Almouzni, G. (2014). Histone chaperones: assisting histone traffic and nucleosome dynamics. Annu. Rev. Biochem. *83*, 487–517.

Hajkova, P., Jeffries, S.J., Lee, C., Miller, N., Jackson, S.P., and Surani, M.A. (2010). Genome-wide reprogramming in the mouse germ line entails the base excision repair pathway. Science *329*, 78–82.

Hödl, M., and Basler, K. (2009). Transcription in the absence of histone H3.3. Curr. Biol. *19*, 1221–1226.

Hoek, M., and Stillman, B. (2003). Chromatin assembly factor 1 is essential and couples chromatin assembly to DNA replication in vivo. Proc. Natl. Acad. Sci. USA *100*, 12183–12188.

Inoue, A., and Zhang, Y. (2014). Nucleosome assembly is required for nuclear pore complex assembly in mouse zygotes. Nat. Struct. Mol. Biol. *21*, 609–616.

Kaneda, M., Okano, M., Hata, K., Sado, T., Tsujimoto, N., Li, E., and Sasaki, H. (2004). Essential role for de novo DNA methyltransferase Dnmt3a in paternal and maternal imprinting. Nature *429*, 900–903.

Kobayashi, H., Sakurai, T., Imai, M., Takahashi, N., Fukuda, A., Yayoi, O., Sato, S., Nakabayashi, K., Hata, K., Sotomaru, Y., et al. (2012). Contribution of intragenic DNA methylation in mouse gametic DNA methylomes to establish oocyte-specific heritable marks. PLoS Genet. *8*, e1002440.

Kraushaar, D.C., Jin, W., Maunakea, A., Abraham, B., Ha, M., and Zhao, K. (2013). Genome-wide incorporation dynamics reveal distinct categories of turnover for the histone variant H3.3. Genome Biol. *14*, R121.

Lan, Z.J., Xu, X., and Cooney, A.J. (2004). Differential oocyte-specific expression of Cre recombinase activity in GDF-9-iCre, Zp3cre, and Msx2Cre transgenic mice. Biol. Reprod. *71*, 1469–1474.

Li, R., and Albertini, D.F. (2013). The road to maturation: somatic cell interaction and self-organization of the mammalian oocyte. Nat. Rev. Mol. Cell Biol. *14*, 141–152.

Lin, C.J., Conti, M., and Ramalho-Santos, M. (2013). Histone variant H3.3 maintains a decondensed chromatin state essential for mouse preimplantation development. Development *140*, 3624–3634.

Lin, C.J., Koh, F.M., Wong, P., Conti, M., and Ramalho-Santos, M. (2014). Hira-mediated H3.3 incorporation is required for DNA replication and ribosomal RNA transcription in the mouse zygote. Dev. Cell *30*, 268–279.

Ljungman, M., and Hanawalt, P.C. (1992). Efficient protection against oxidative DNA damage in chromatin. Mol. Carcinog. *5*, 264–269.

Loppin, B., Bonnefoy, E., Anselme, C., Laurençon, A., Karr, T.L., and Couble, P. (2005). The histone H3.3 chaperone HIRA is essential for chromatin assembly in the male pronucleus. Nature *437*, 1386–1390.

Maze, I., Noh, K.M., Soshnev, A.A., and Allis, C.D. (2014). Every amino acid matters: essential contributions of histone variants to mammalian development and disease. Nat. Rev. Genet. *15*, 259–271.

Maze, I., Wenderski, W., Noh, K.M., Bagot, R.C., Tzavaras, N., Purushothaman, I., Elsässer, S.J., Guo, Y., Ionete, C., Hurd, Y.L., et al. (2015). Critical Role of Histone Turnover in Neuronal Transcription and Plasticity. Neuron *87*, 77–94.

Mito, Y., Henikoff, J.G., and Henikoff, S. (2005). Genome-scale profiling of histone H3.3 replacement patterns. Nat. Genet. *37*, 1090–1097.

Nashun, B., Yukawa, M., Liu, H., Akiyama, T., and Aoki, F. (2010). Changes in the nuclear deposition of histone H2A variants during pre-implantation development in mice. Development *137*, 3785–3794.

Pan, H., O'brien, M.J., Wigglesworth, K., Eppig, J.J., and Schultz, R.M. (2005). Transcript profiling during mouse oocyte development and the effect of gonadotropin priming and development in vitro. Dev. Biol. *286*, 493–506.

Pchelintsev, N.A., McBryan, T., Rai, T.S., van Tuyn, J., Ray-Gallet, D., Almouzni, G., and Adams, P.D. (2013). Placing the HIRA histone chaperone complex in the chromatin landscape. Cell Rep. *3*, 1012–1019.

Polo, S.E., Roche, D., and Almouzni, G. (2006). New histone incorporation marks sites of UV repair in human cells. Cell *127*, 481–493.

Ransom, M., Dennehey, B.K., and Tyler, J.K. (2010). Chaperoning histones during DNA replication and repair. Cell *140*, 183–195.

Ray-Gallet, D., Quivy, J.P., Scamps, C., Martini, E.M.D., Lipinski, M., and Almouzni, G. (2002). HIRA is critical for a nucleosome assembly pathway independent of DNA synthesis. Mol. Cell *9*, 1091–1100.

Sakai, A., Schwartz, B.E., Goldstein, S., and Ahmad, K. (2009). Transcriptional and developmental functions of the H3.3 histone variant in Drosophila. Curr. Biol. *19*, 1816–1820.

Santenard, A., Ziegler-Birling, C., Koch, M., Tora, L., Bannister, A.J., and Torres-Padilla, M.E. (2010). Heterochromatin formation in the mouse embryo requires critical residues of the histone variant H3.3. Nat. Cell Biol. *12*, 853–862.

Shirane, K., Toh, H., Kobayashi, H., Miura, F., Chiba, H., Ito, T., Kono, T., and Sasaki, H. (2013). Mouse oocyte methylomes at base resolution reveal genome-wide accumulation of non-CpG methylation and role of DNA methyltransferases. PLoS Genet. *9*, e1003439.

Smallwood, S.A., and Kelsey, G. (2012). De novo DNA methylation: a germ cell perspective. Trends Genet. *28*, 33–42.

Smallwood, S.A., Tomizawa, S., Krueger, F., Ruf, N., Carli, N., Segonds-Pichon, A., Sato, S., Hata, K., Andrews, S.R., and Kelsey, G. (2011). Dynamic CpG island methylation landscape in oocytes and preimplantation embryos. Nat. Genet. *43*, 811–814.

Smallwood, S.A., Lee, H.J., Angermueller, C., Krueger, F., Saadeh, H., Peat, J., Andrews, S.R., Stegle, O., Reik, W., and Kelsey, G. (2014). Single-cell genome-wide bisulfite sequencing for assessing epigenetic heterogeneity. Nat. Methods *11*, 817–820.

Tagami, H., Ray-Gallet, D., Almouzni, G., and Nakatani, Y. (2004). Histone H3.1 and H3.3 complexes mediate nucleosome assembly pathways dependent or independent of DNA synthesis. Cell *116*, 51–61.

Tang, M.C., Jacobs, S.A., Mattiske, D.M., Soh, Y.M., Graham, A.N., Tran, A., Lim, S.L., Hudson, D.F., Kalitsis, P., O'Bryan, M.K., et al. (2015). Contribution of the two genes encoding histone variant h3.3 to viability and fertility in mice. PLoS Genet. *11*, e1004964.

Teves, S.S., Weber, C.M., and Henikoff, S. (2014). Transcribing through the nucleosome. Trends Biochem. Sci. *39*, 577–586.

Tomizawa, S., Nowacka-Woszuk, J., and Kelsey, G. (2012). DNA methylation establishment during oocyte growth: mechanisms and significance. Int. J. Dev. Biol. *56*, 867–875.

Trapnell, C., Williams, B.A., Pertea, G., Mortazavi, A., Kwan, G., van Baren, M.J., Salzberg, S.L., Wold, B.J., and Pachter, L. (2010). Transcript assembly and quantification by RNA-Seq reveals unannotated transcripts and isoform switching during cell differentiation. Nat. Biotechnol. *28*, 511–515.

Veselovska, L., Smallwood, S.A., Saadeh, H., Stewart, K.R., Krueger, F., Maupetit-Méhouas, S., Arnaud, P., Tomizawa, S., Andrews, S., and Kelsey, G. (2015). Deep sequencing and de novo assembly of the mouse oocyte transcriptome define the contribution of transcription to the DNA methylation landscape. Genome Biol. *16*, 209.

Wirbelauer, C., Bell, O., and Schübeler, D. (2005). Variant histone H3.3 is deposited at sites of nucleosomal displacement throughout transcribed genes while active histone modifications show a promoter-proximal bias. Genes Dev. *19*, 1761–1766.

Wyrick, J.J., Holstege, F.C., Jennings, E.G., Causton, H.C., Shore, D., Grunstein, M., Lander, E.S., and Young, R.A. (1999). Chromosomal landscape of nucleosome-dependent gene expression and silencing in yeast. Nature *402*, 418–421.

Yang, X., Han, H., De Carvalho, D.D., Lay, F.D., Jones, P.A., and Liang, G. (2014). Gene body methylation can alter gene expression and is a therapeutic target in cancer. Cancer Cell *26*, 577–590.

Molecular Cell, Volume *60*

Supplemental Information

Continuous Histone Replacement by Hira Is Essential for Normal Transcriptional Regulation and De Novo DNA Methylation during Mouse Oogenesis

Buhe Nashun, Peter W.S. Hill, Sebastien A. Smallwood, Gopuraja Dharmalingam, Rachel Amouroux, Stephen J. Clark, Vineet Sharma, Elodie Ndjetehe, Pawel Pelczar, Richard J. Festenstein, Gavin Kelsey, and Petra Hajkova

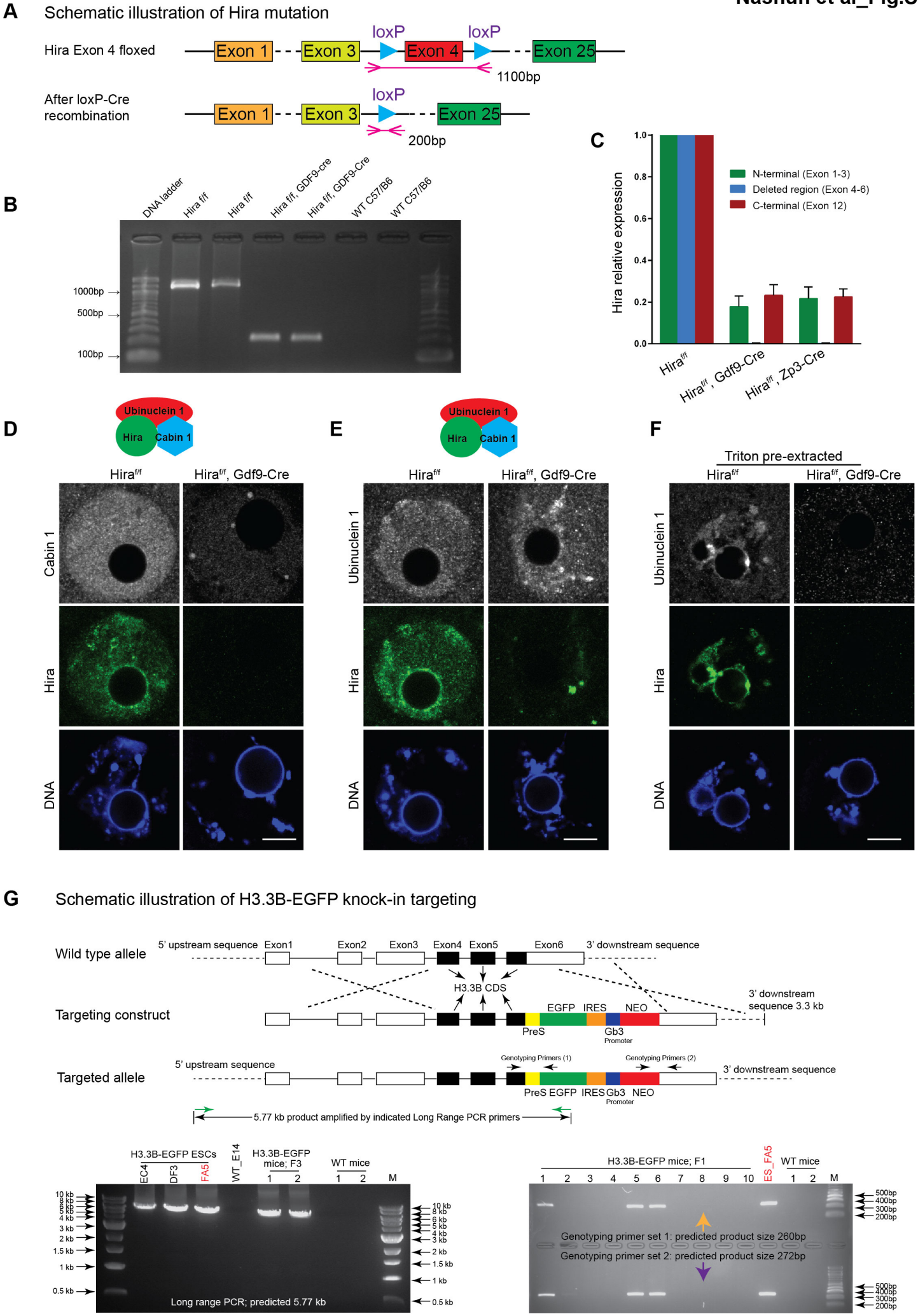
A
Schematic illustration of Hira mutation
Hira Exon 4 floxed
Exon 1
Exon 3
loxP
Exon 4
loxP
Exon 25
1100bp
After loxP-Cre recombination
Exon 1
Exon 3
loxP
Exon 25
200bp
B
DNA ladder
Hira f/f
Hira f/f
Hira f/f, GDF9-cre
Hira f/f, GDF9-Cre
WT C57/B6
WT C57/B6
1000bp
500bp
100bp
C
Hira relative expression
1.0
0.8
0.6
0.4
0.2
0.0
N-terminal (Exon 1-3)
Deleted region (Exon 4-6)
C-terminal (Exon 12)
Hira f/f
Hira f/f, Gdf9-Cre
Hira f/f, Zp3-Cre
D
Ubinuclein 1
Hira
Cabin 1
Hira f/f
Hira f/f, Gdf9-Cre
Cabin 1
Hira
DNA
E
Ubinuclein 1
Hira
Cabin 1
Hira f/f
Hira f/f, Gdf9-Cre
Ubinuclein 1
Hira
DNA
F
Triton pre-extracted
Hira f/f
Hira f/f, Gdf9-Cre
Ubinuclein 1
Hira
DNA
G
Schematic illustration of H3.3B-EGFP knock-in targeting
Wild type allele
5' upstream sequence
Exon1
Exon2
Exon3
Exon4
Exon5
Exon6
3' downstream sequence
H3.3B CDS
Targeting construct
EGFP
IRES
NEO
3' downstream sequence 3.3 kb
PreS
Gb3 Promoter
Targeted allele
5' upstream sequence
Genotyping Primers (1)
Genotyping Primers (2)
3' downstream sequence
PreS EGFP IRES Gb3 Promoter NEO
5.77 kb product amplified by indicated Long Range PCR primers
H3.3B-EGFP ESCs
EC4
DF3
FA5
WT_E14
H3.3B-EGFP mice; F3
1
2
WT mice
1
2
M
10 kb
8 kb
6 kb
5 kb
4 kb
3 kb
2 kb
1.5 kb
1 kb
0.5 kb
Long range PCR; predicted 5.77 kb
H3.3B-EGFP mice; F1
1 2 3 4 5 6 7 8 9 10
ES_FA5
WT mice
1 2
M
500bp
400bp
300bp
200bp
Genotyping primer set 1: predicted product size 260bp
Genotyping primer set 2: predicted product size 272bp

Figure S1. Oocyte specific depletion of Hira, related to Figure 1.

(A) Schematic illustration of Hira locus targeting. (B) PCR genotyping confirming genetic recombination in *Hira*$^{f/f}$, *Gdf9-Cre*$^{+}$ GV stage oocytes. (C) qPCR detection of *Hira* mRNA expression levels in zygotes from *Hira*$^{f/f}$, *Hira*$^{f/f}$ *Gdf9-Cre*$^{+}$ or *Hira*$^{f/f}$ *Zp3-Cre*$^{+}$ (oocytes fertilized by wild type sperm). The expression was normalized to exogenous RNA standard and set as 1 in *Hira*$^{f/f}$ zygotes. Error bars indicate s.e.m of three independent experiments. (D-F) CABIN1 (D) or UBN1 (E, F) staining in GV stage oocytes from *Hira*$^{f/f}$ or *Hira*$^{f/f}$ *Gdf9-Cre*$^{+}$ females. Note that CABIN1 was mostly depleted in Hira mutant oocytes (D) and residual amount of UBN1 (E) disappeared after Triton pre-extraction suggesting lack of chromatin association in the absence of Hira (F). DNA was stained with DAPI and shown in blue. Scale bar=10 μm. (G) Schematic illustration of H3.3B-EGFP knock-in targeting and the genotyping results.

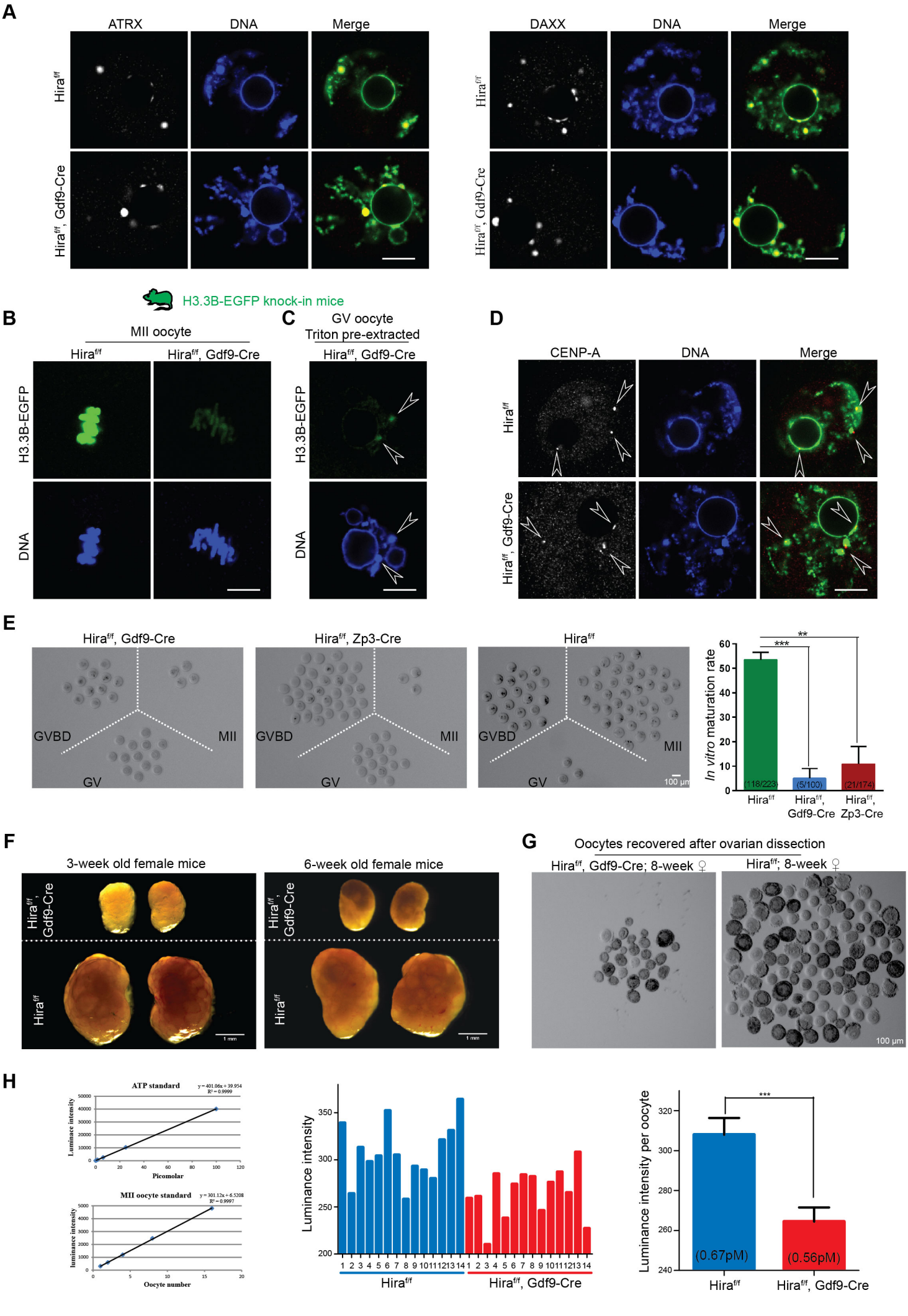
A
ATRX
DNA
Merge
DAXX
DNA
Merge
Hira f/f
Hira f/f, Gdf9-Cre
H3.3B-EGFP knock-in mice
B
MII oocyte
Hira f/f
Hira f/f, Gdf9-Cre
H3.3B-EGFP
DNA
C
GV oocyte
Triton pre-extracted
Hira f/f, Gdf9-Cre
H3.3B-EGFP
DNA
D
CENP-A
DNA
Merge
Hira f/f
Hira f/f, Gdf9-Cre
E
Hira f/f, Gdf9-Cre
Hira f/f, Zp3-Cre
Hira f/f
GVBD
MII
GV
100 μm
In vitro maturation rate
(118/223)
(5/100)
(21/174)
Hira f/f
Hira f/f, Gdf9-Cre
Hira f/f, Zp3-Cre
F
3-week old female mice
6-week old female mice
Hira f/f, Gdf9-Cre
Hira f/f
1 mm
G
Oocytes recovered after ovarian dissection
Hira f/f, Gdf9-Cre; 8-week ♀
Hira f/f; 8-week ♀
100 μm
H
ATP standard
Luminance intensity
Picomolar
MII oocyte standard
Oocyte number
Luminance intensity
Hira f/f
Hira f/f, Gdf9-Cre
Luminance intensity per oocyte
(0.67pM)
(0.56pM)
Hira f/f
Hira f/f, Gdf9-Cre

Figure S2. Effects of Hira deletion on oocyte development, histone incorporation and on ATRX/DAXX, an alternative H3.3 chaperone complex, related to Figure 1 and Figure 2.

(A) Maternal Hira depletion did not affect ATRX/DAXX localisation in GV oocytes. (B) Residual H3.3B-EGFP signal could be detected in the MII chromosome in oocytes obtained from *Hira*$^{f/f}$ *Gdf9-Cre*$^{+}$, H3.3B-EGFP mice , the signal is greatly reduced compared to the control. (C) Residual foci of chromatin associated H3.3 (indicated by arrowheads) were detected in Triton pre-extracted *Hira*$^{f/f}$ *Gdf9-Cre*$^{+}$, H3.3B-EGFP GV oocytes following laser intensity enhancement. (D) CENP-A distribution (indicated by arrowheads) was not affected by maternal Hira depletion. DNA was stained with DAPI and shown in blue. Scale bar=10 μm (E) Meiotic competence is greatly reduced in Hira depleted oocytes. GV oocytes were recovered from 3 week old *Hira*$^{f/f}$, *Hira*$^{f/f}$ *Gdf9-Cre*$^{+}$ or *Hira*$^{f/f}$ *Zp3-Cre*$^{+}$ females and cultured for 16 hours. Meiotic maturation was judged by the first polar body extrusion. Representative bright field images of the oocytes after overnight incubation are shown on the left; quantification graph is shown on the right. (F) Representative images of three independent experiments showing ovaries of *Hira*$^{f/f}$ or *Hira*$^{f/f}$ *Gdf9-Cre*$^{+}$ siblings at 3 or 6 weeks of age. Images were taken in a single picture. (G) Representative images of oocytes recovered after ovarian dissection of 8 week old *Hira*$^{f/f}$ or *Hira*$^{f/f}$ *Gdf9-Cre*$^{+}$ siblings. Dissections were carried out twice at 8 week and twice at 5 week old stages (data not shown). Scale bars as indicated. (H) Quantification of ATP levels in single MII oocytes. Standard curve for ATP of oocytes is shown on the left. Luminance intensity of single MII oocyte ATP level (middle). 14 MII oocytes collected from two *Hira*$^{f/f}$ or two *Hira*$^{f/f}$ *Gdf9-Cre*$^{+}$ females were subjected to ATP measurement. Quantification of average level of ATP content in single MII oocytes (right). Absolute ATP content was calculated using the standard curves and indicated in each column. In all cases, error bars indicate s.e.m.; ns, non-significant; *, $p<0.05$; **, $p<0.01$; ***, $p<0.001$.

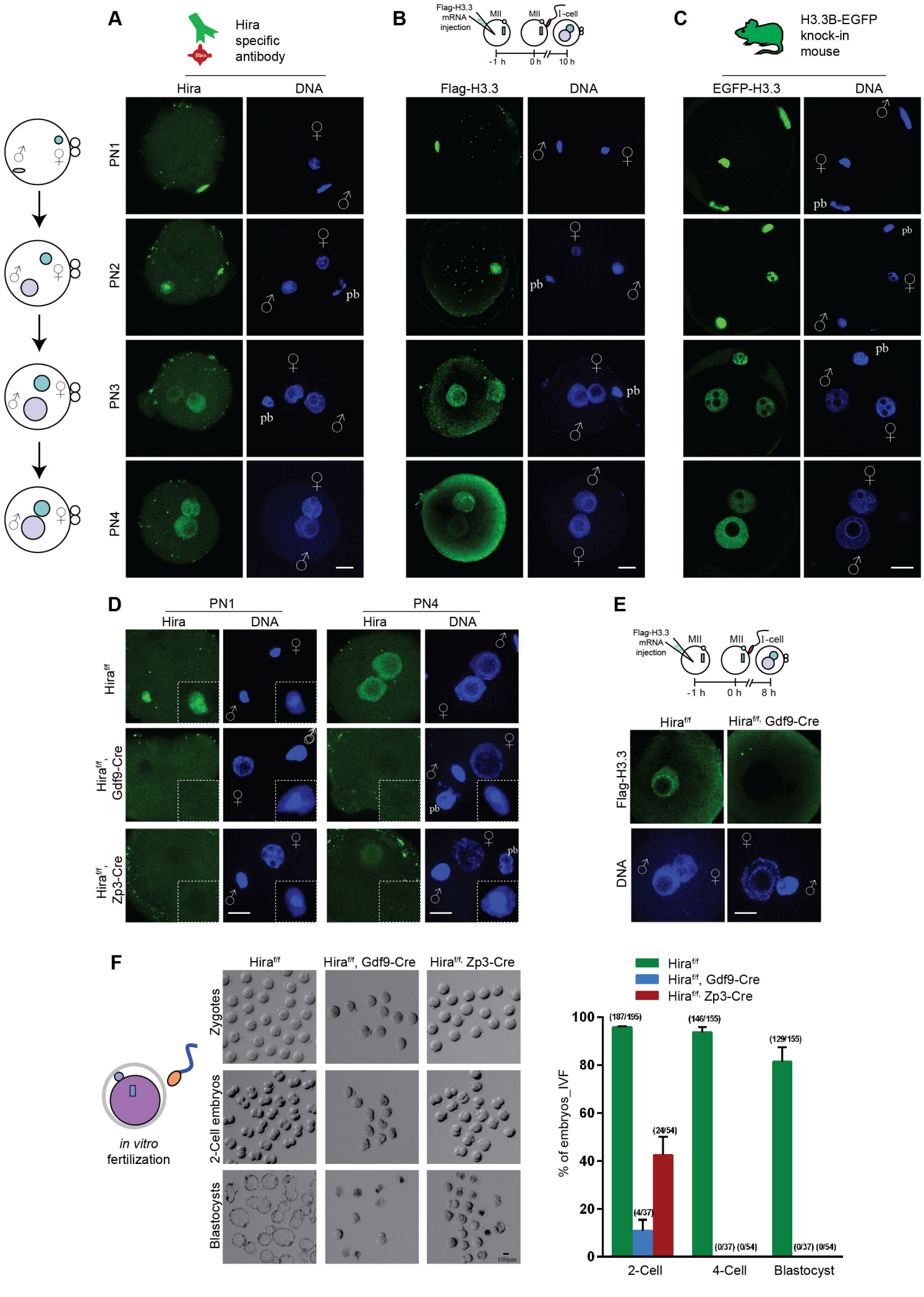
A
Hira specific antibody
Hira
DNA
PN1
PN2
PN3
PN4
pb
B
Flag-H3.3 mRNA injection
MII
MII
1-cell
-1 h
0 h
10 h
Flag-H3.3
DNA
C
H3.3B-EGFP knock-in mouse
EGFP-H3.3
DNA
D
PN1
PN4
Hira
DNA
Hira f/f
Hira f/f, Gdf9-Cre
Hira f/f, Zp3-Cre
E
Flag-H3.3 mRNA injection
MII
MII
1-cell
-1 h
0 h
8 h
Hira f/f
Hira f/f, Gdf9-Cre
Flag-H3.3
DNA
F
Hira f/f
Hira f/f, Gdf9-Cre
Hira f/f, Zp3-Cre
Zygotes
2-Cell embryos
Blastocysts
100μm
in vitro fertilization
% of embryos_IVF
100
80
60
40
20
0
(187/195)
(4/37)
(24/54)
(146/155)
(0/37)
(0/54)
(129/155)
(0/37)
(0/54)
2-Cell
4-Cell
Blastocyst

Figure S3. Maternal Hira is necessary for H3.3 incorporation in zygotes, related to Figure 2.

(A) Localisation of Hira during mouse zygotic development. (B) H3.3 incorporation in mouse zygotes following microinjection of Flag-H3.3 mRNA. Zygotes were fixed at different PN stages and stained with anti-Flag antibody. (C) H3.3B-EGFP distribution in mouse zygotes. MII oocytes were collected from 3-week old *H3.3B-EGFP* knock-in females and fertilised *in vitro* by wild type sperm. Zygotes were fixed at different PN stages and stained with anti-GFP antibody. (D) Hira protein is completely absent from zygotes obtained by *in vitro* fertilisation of *Hira*$^{f/f}$ *Gdf9-Cre*$^{+}$ or *Hira*$^{f/f}$ *Zp3-Cre*$^{+}$ MII oocytes with wild type sperm. An enlarged image of paternal pronucleus is shown in the insets. Note that paternal genome underwent only partial de-condensation. (E) Maternal Hira is necessary for H3.3 incorporation into the paternal pronucleus. *Hira*$^{f/f}$ or *Hira*$^{f/f}$ *Gdf9-Cre*$^{+}$ MII oocytes were microinjected with Flag-H3.3 mRNA and *in vitro* fertilised by wild type sperm. Zygotes were fixed and stained by anti-Flag antibody 8 hours later. (F) Early developmental arrest of embryos with maternal Hira depletion. MII oocytes were collected from *Hira*$^{f/f}$, *Hira*$^{f/f}$ *Gdf9-Cre*$^{+}$ or *Hira*$^{f/f}$ *Zp3-Cre*$^{+}$ females following hormonal stimulation and fertilised *in vitro* by wild type sperm prior to *in vitro* culture. Representative images of embryos (left panel); quantification of developmental progression (right panel). Embryo numbers are indicated above each column. Zygotes depleted of Hira do not progress beyond the two-cell stage. DNA is stained by DAPI (blue). ♀, female pronucleus; ♂, male pronucleus; pb, polar body. Scale bar= 10μm

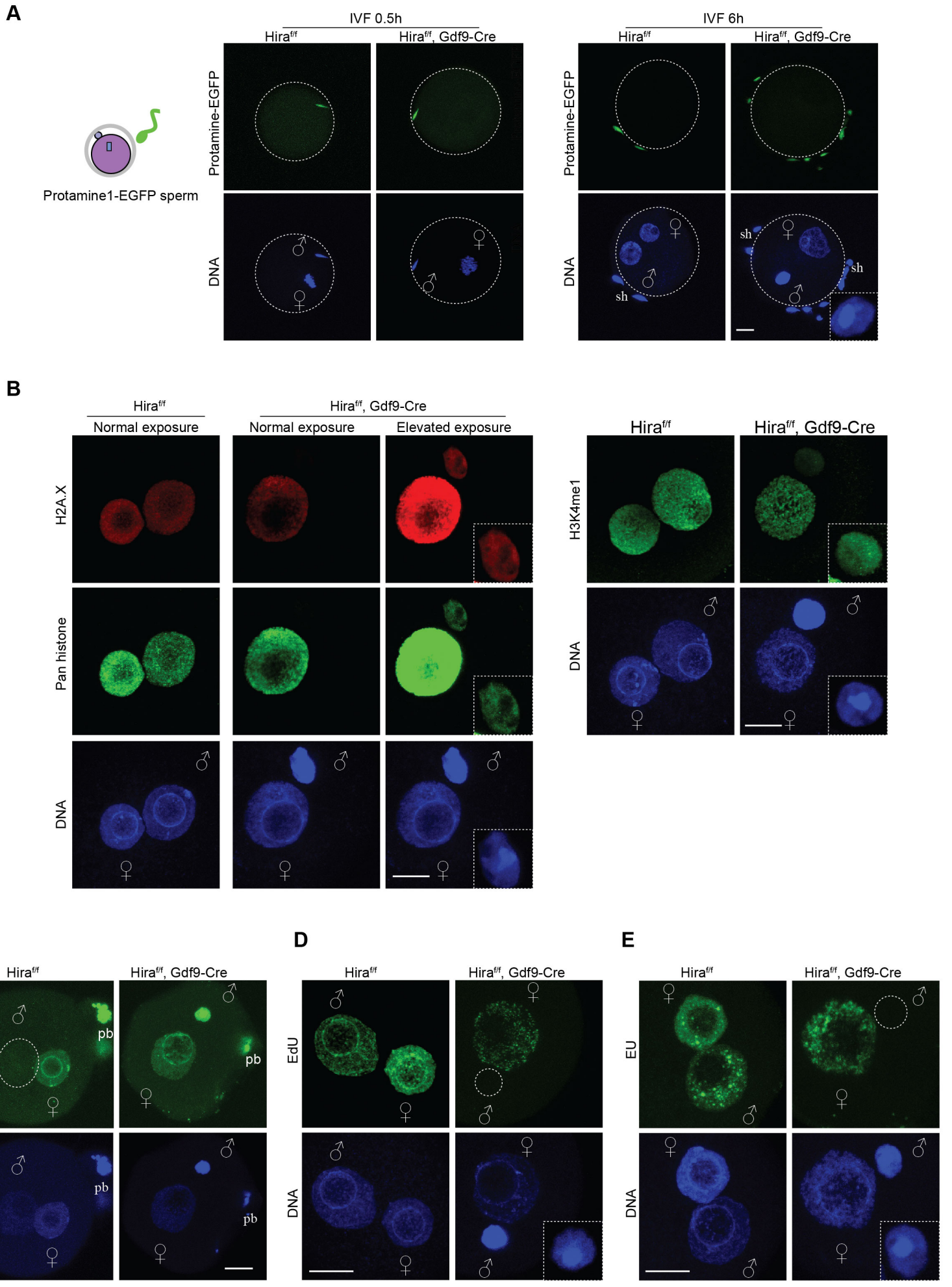
A
IVF 0.5h
IVF 6h
Hira f/f
Hira f/f, Gdf9-Cre
Protamine-EGFP
DNA
Protamine1-EGFP sperm
sh
B
Hira f/f
Hira f/f, Gdf9-Cre
Normal exposure
Elevated exposure
H2A.X
Pan histone
H3K4me1
C
5mC
pb
D
EdU
E
EU

Figure S4. Maternal Hira depleted oocytes fail to reprogramme paternal genome after fertilisation, related to Figure 2.

(A) Protamine removal is not affected by maternal Hira depletion. MII ooyctes collected from *Hira*$^{f/f}$ *Gdf9-Cre*$^{+}$ females were fertilized *in vitro* by sperm collected from *protamine1-EGFP* transgenic adult male mice. Zygotes were fixed at the indicated time points. Note that protamines were detectable in the paternal genome 0.5h after insemination but were not detectable afterwards. Sperm heads, which could not enter the oocyte, were used as positive control for Protamine 1 staining. Oocytes from *Hira* $^{f/f}$ siblings were used as control. (B) Paternal pronucleus of zygotes maternally depleted for Hira contains residual histones. *Hira*$^{f/f}$ or *Hira*$^{f/f}$ *Gdf9-Cre*$^{+}$ oocytes were fertilised *in vitro* by wild type sperm. The zygotes were fixed 10 hours later and simultaneously stained with anti-H2A.X, anti-pan histone antibodies (left) or for the presence of H3K4me1 (right). (C) DNA demethylation did not occur in the partially decondensed paternal genome of Hira mutant zygote. MII oocytes obtained from *Hira*$^{f/f}$ or *Hira*$^{f/f}$ *Gdf9-Cre*$^{+}$ females were fertilised *in vitro* by wild type sperm. The zygotes were fixed at PN4-5 stages and stained with anti-5mC antibody. DNA was stained by PI and pseudocoloured in blue. (D, E) Representative images for detection of DNA replication by EdU labelling (D) or of nascent RNA synthesis by EU labelling (E). MII oocytes collected from *Hira*$^{f/f}$ or *Hira*$^{f/f}$ *Gdf9-Cre*$^{+}$ siblings were fertilized *in vitro* by wild type sperm and cultured in presence of EdU (D) or EU (E) and fixed at PN4-5 stage. Note that neither replication nor transcription was detected in the partially decondensed paternal pronucleus in maternal Hira deleted zygotes. Enlarged image of paternal pronucleus is shown in the inset (b,d,e). ♀, female pronucleus; ♂, male pronucleus; pb, polar body. sh, sperm head. Scale bar= 10 μm

A

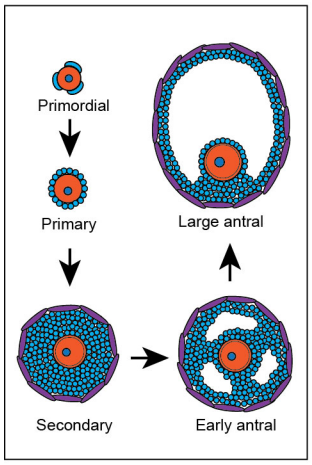
Primordial
Primary
Large antral
Secondary
Early antral

C

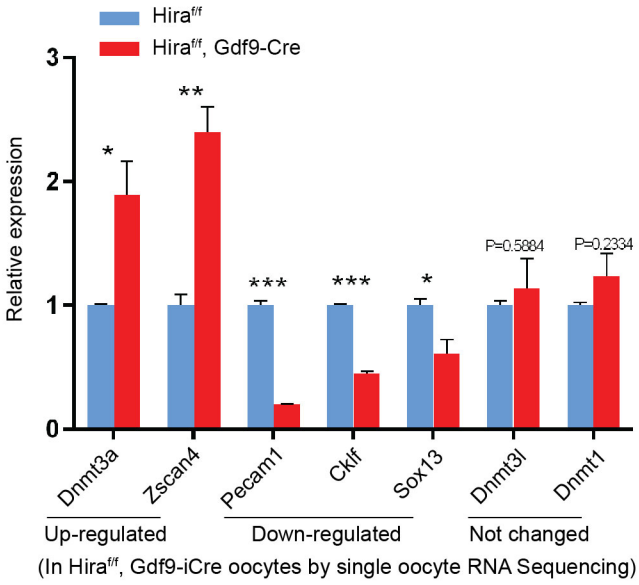
Hira$^{f/f}$
Hira$^{f/f}$, Gdf9-Cre
Relative expression
3
2
1
0
*
**
***
***
*
P=0.5884
P=0.2334
Dnmt3a
Zscan4
Pecam1
Cklf
Sox13
Dnmt3l
Dnmt1
Up-regulated
Down-regulated
Not changed
(In Hira$^{f/f}$, Gdf9-iCre oocytes by single oocyte RNA Sequencing)

B

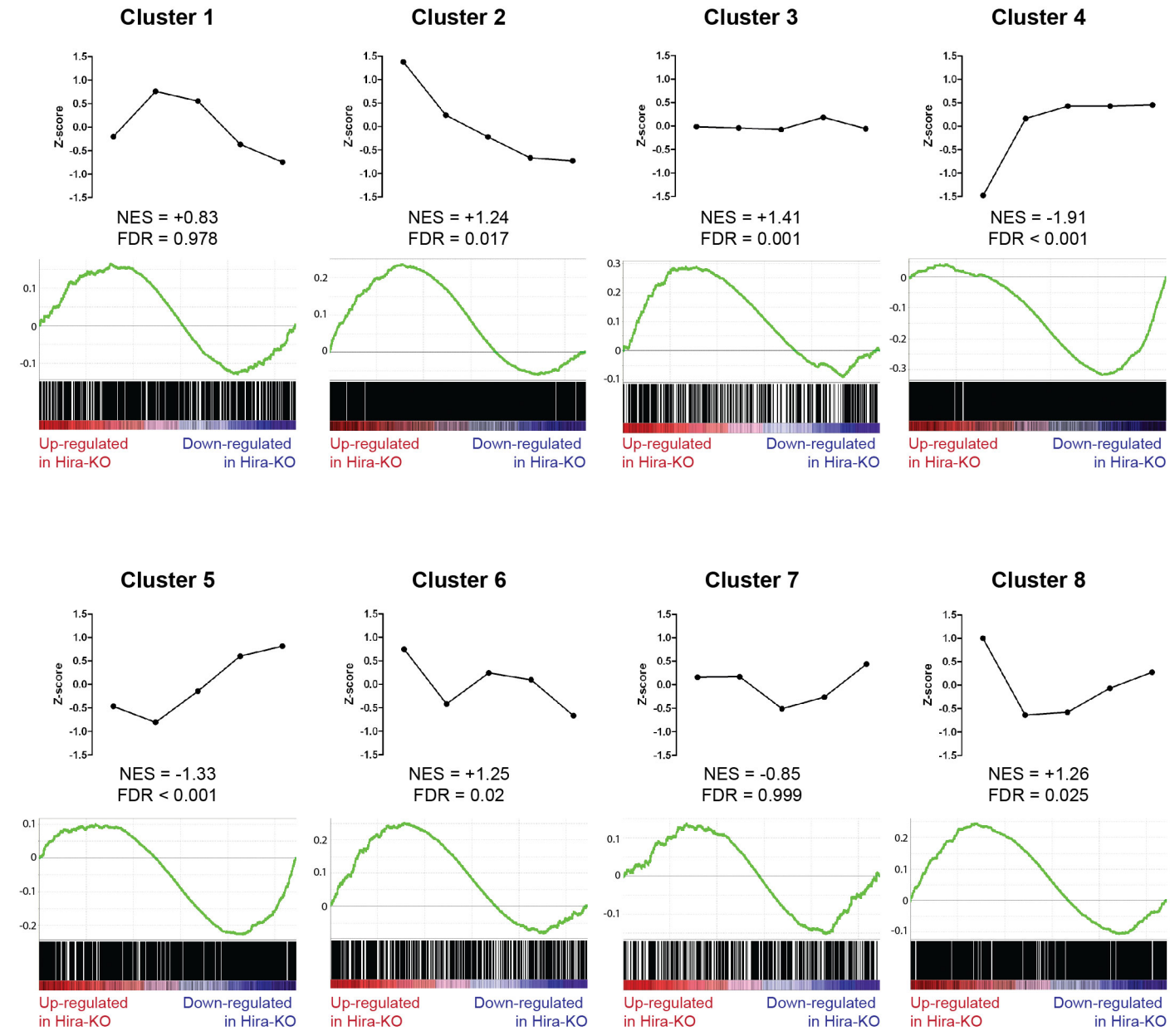
Cluster 1
NES = +0.83
FDR = 0.978
Cluster 2
NES = +1.24
FDR = 0.017
Cluster 3
NES = +1.41
FDR = 0.001
Cluster 4
NES = -1.91
FDR < 0.001
Cluster 5
NES = -1.33
FDR < 0.001
Cluster 6
NES = +1.25
FDR = 0.02
Cluster 7
NES = -0.85
FDR = 0.999
Cluster 8
NES = +1.26
FDR = 0.025
Z-score
Up-regulated in Hira-KO
Down-regulated in Hira-KO

Figure S5. Relationship between gene expression changes in Hira depleted oocytes and transcriptional dynamics during oogenesis, related to Figure 5.

(A) Schematic illustration of developmental stages during oogenesis. Adapted from previous publications (Li and Albertini, 2013; Pan et al., 2005). (B) Gene set enrichment analysis (GSEA) comparing gene expression patterns during oogenesis (Pan et al., 2005) and the ranked list of gene expression changes in *Hira*$^{f/f}$ *Gdf9-Cre*$^{+}$ relative to *Hira*$^{f/f}$ MII oocytes. NES - Normalised Enrichment Score; FDR – False Discovery Rate (calculated in GSEA program). For each cluster, each dot represents mean-normalised gene expression for consecutive stages of oocyte development. (C) qPCR validation of Hira$^{f/f}$, GDF9-Cre^{+} single oocyte RNA sequencing. A range of genes were selected from RNA sequencing data and the expression was normalized to exogenous RNA standard and set as 1 in *Hira*$^{f/f}$ zygotes. Error bars indicate s.e.m of three technical replicates.

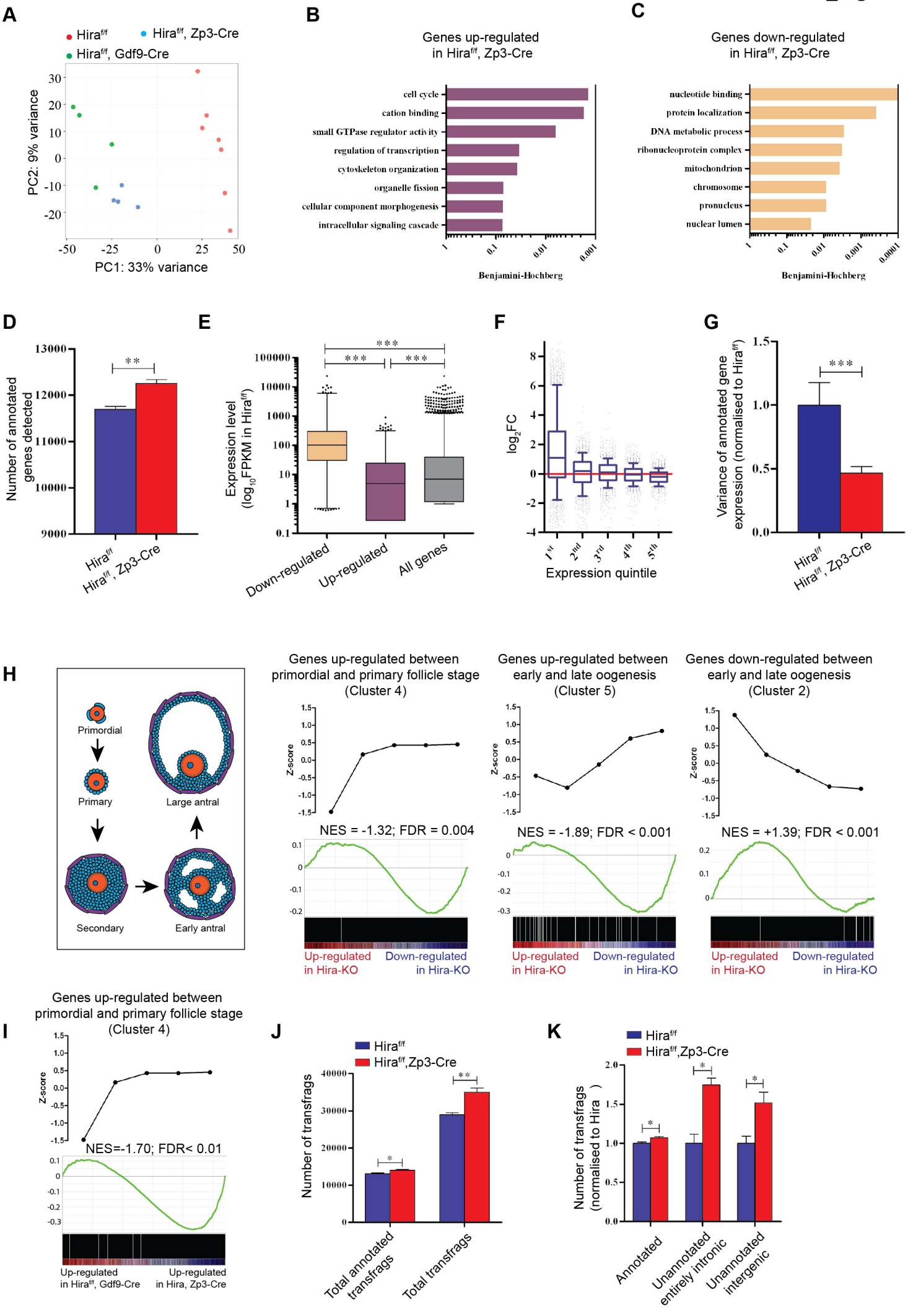
A
Hira f/f
Hira f/f, Zp3-Cre
Hira f/f, Gdf9-Cre
PC2: 9% variance
PC1: 33% variance
B
Genes up-regulated in Hira f/f, Zp3-Cre
cell cycle
cation binding
small GTPase regulator activity
regulation of transcription
cytoskeleton organization
organelle fission
cellular component morphogenesis
intracellular signaling cascade
Benjamini-Hochberg
C
Genes down-regulated in Hira f/f, Zp3-Cre
nucleotide binding
protein localization
DNA metabolic process
ribonucleoprotein complex
mitochondrion
chromosome
pronucleus
nuclear lumen
Benjamini-Hochberg
D
Number of annotated genes detected
Hira f/f
Hira f/f, Zp3-Cre
E
Expression level (log10FPKM in Hira f/f)
Down-regulated
Up-regulated
All genes
F
log2FC
Expression quintile
G
Variance of annotated gene expression (normalised to Hira f/f)
Hira f/f
Hira f/f, Zp3-Cre
H
Primordial
Primary
Large antral
Secondary
Early antral
Genes up-regulated between primordial and primary follicle stage (Cluster 4)
Z-score
NES = -1.32; FDR = 0.004
Up-regulated in Hira-KO
Down-regulated in Hira-KO
Genes up-regulated between early and late oogenesis (Cluster 5)
NES = -1.89; FDR < 0.001
Genes down-regulated between early and late oogenesis (Cluster 2)
NES = +1.39; FDR < 0.001
I
Genes up-regulated between primordial and primary follicle stage (Cluster 4)
NES=-1.70; FDR< 0.01
Up-regulated in Hira f/f, Gdf9-Cre
Up-regulated in Hira, Zp3-Cre
J
Hira f/f
Hira f/f,Zp3-Cre
Number of transfrags
Total annotated transfrags
Total transfrags
K
Hira f/f
Hira f/f,Zp3-Cre
Number of transfrags (normalised to Hira)
Annotated
Unannotated entirely intronic
Unannotated intergenic

Figure S6. Hira$^{f/f}$, Zp3-Cre^{+} Single Oocyte RNA sequencing, related to Figure 4 and Figure 5.

(A) PCA plot of scRNA-Seq data derived from *Hira*$^{f/f}$, *Hira*$^{f/f}$ *Gdf9-Cre*$^{+}$, and *Hira*$^{f/f}$ *Zp3-Cre*$^{+}$ MII oocytes; PC1 and PC2 refer to the first and second principle components, respectively. Hira-wild type and Hira-knockout oocytes are clearly distinguishable by PC1 (note: Hira$^{f/f}$ samples were used to correct for batch effect). (B, C) Selected gene ontology (GO) terms significantly enriched for among differentially up-regulated (B, EdgeR, FDR < 0.1) and differentially down-regulated (C, EdgeR, FDR < 0.1) genes in *Hira*$^{f/f}$ *Zp3-Cre*$^{+}$ MII oocytes. X-axis represents the Benjamini-Hochberg adjusted p value. (D) Number of annotated genes detected, as computed by HTSeq programme. (E) Boxplot of gene expression levels of differentially up- or down-regulated genes between *Hira*$^{f/f}$ *Zp3-Cre*$^{+}$ and *Hira*$^{f/f}$ MII oocytes (EdgeR, FDR < 0.1), and all annotated genes. (F) Box plots showing distribution of gene expression fold-change for each gene expression level quintile (based on *Hira*$^{f/f}$ gene-expression levels). (G) Variance of gene expression within a given *Hira*$^{f/f}$ or *Hira*$^{f/f}$ *Zp3-Cre*$^{+}$ sample. (H) Gene set enrichment analysis (GSEA) comparing genes of selected expression clusters during oogenesis (Figure S6) and the ranked list of gene expression changes in *Hira*$^{f/f}$ *Zp3-Cre*$^{+}$ MII oocytes relative to *Hira*$^{f/f}$ oocytes. NES - Normalised Enrichment Score; FDR - False Discovery Rate (both calculated in GSEA program). For each cluster, each dot represents mean-normalised gene expression for consecutive stages of oocyte development. (I) GSEA comparing genes of cluster 4 (i.e. specifically up-regulated between primordial and primary stages) and the ranked list of gene expression changes in *Hira*$^{f/f}$ *Gdf9-Cre*$^{+}$ MII oocytes relative to and *Hira*$^{f/f}$ *Zp3-Cre*$^{+}$ MII oocytes. NES - Normalised Enrichment Score; FDR - False Discovery Rate (both calculated in GSEA program). (J) Number of total transfrags and total annotated transfrags in *Hira*$^{f/f}$ and *Hira*$^{f/f}$ *Zp3-Cre*$^{+}$ MII oocytes (as computed by CuffCompare program). (K) Number of total annotated transfrags, unannotated

entirely intronic transfrags, and unannotated entirely intergenic transfrags in *Hira*$^{f/f}$ and *Hira*$^{f/f}$ *Zp3-Cre*$^{+}$ MII oocytes (as computed by CuffCompare program). In all cases error bars indicate s.e.m.; ns, non-significant; *, $p<0.05$; **, $p<0.01$; ***, $p<0.001$. Statistical analysis was carried out using two-tailed unpaired Student's t-test (D, I, J), Kruskal-Wallis with Dunn's post-hoc test (E) or F-test (G).

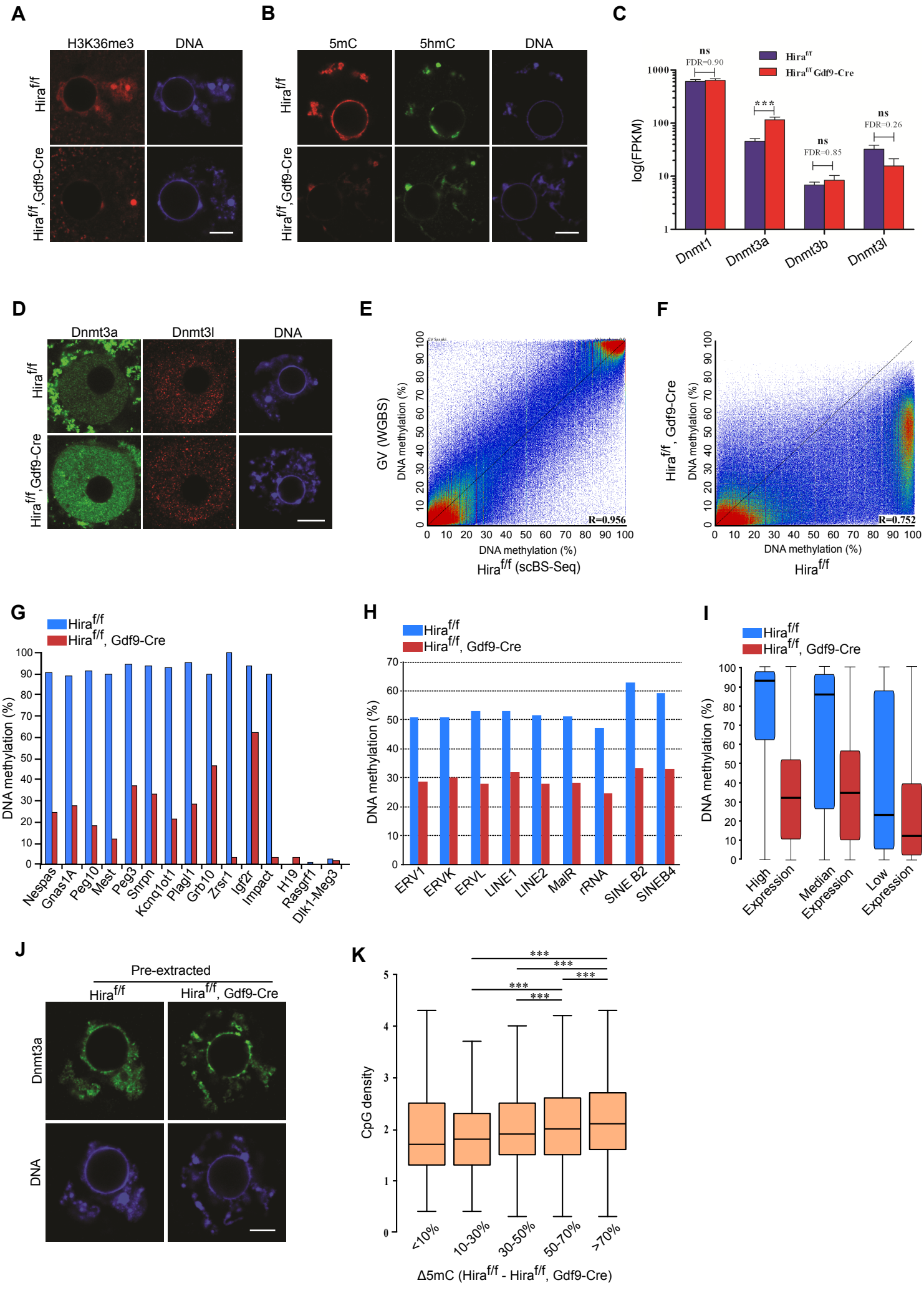
A
H3K36me3
DNA
Hira f/f
Hira f/f,Gdf9-Cre
B
5mC
5hmC
DNA
C
ns
FDR=0.90
***
ns
FDR=0.85
ns
FDR=0.26
Hira f/f
Hira f/f Gdf9-Cre
log(FPKM)
Dnmt1
Dnmt3a
Dnmt3b
Dnmt3l
D
Dnmt3a
Dnmt3l
DNA
E
GV (WGBS)
DNA methylation (%)
R=0.956
Hira f/f (scBS-Seq)
F
Hira f/f, Gdf9-Cre
R=0.752
G
Hira f/f
Hira f/f, Gdf9-Cre
DNA methylation (%)
Nespas
Gnas1A
Peg10
Mest
Peg3
Snrpn
Kcnq1ot1
Plagl1
Grb10
Zrsr1
Igf2r
Impact
H19
Rasgrf1
Dlk1-Meg3
H
ERV1
ERVK
ERVL
LINE1
LINE2
MalR
rRNA
SINE B2
SINEB4
I
High Expression
Median Expression
Low Expression
J
Pre-extracted
Dnmt3a
DNA
K
CpG density
<10%
10-30%
30-50%
50-70%
>70%
Δ5mC (Hira f/f - Hira f/f, Gdf9-Cre)

Figure S7. Further characterisation of global DNA hypomethylation observed in Hira depleted oocytes, related to Figure 6.

(A) Global H3K36me3 levels are lower in *Hira*$^{f/f}$, *Gdf9-Cre*$^{+}$ oocytes as judged by immunofluorescence staining. (B) Immunofluorescence staining showing the reduction of global 5-methylcytosine (5mC) and comparable level of 5-hydroxymethylcytosine (5hmC) in *Hira*$^{f/f}$ and *Hira*$^{f/f}$, *Gdf9-Cre*$^{+}$ GV oocyte. (C) Expression levels of DNA methyltransferases in *Hira*$^{f/f}$ and *Hira*$^{f/f}$, *Gdf9-Cre*$^{+}$; False Discovery Rate (FDR) was computed by the edgeR programme. (D) Immunofluorescence staining of Dnmt3a and Dnmt3l. Note the elevated levels of Dnmt3a and comparable level of Dnmt3l in *Hira*$^{f/f}$, *Gdf9-Cre*$^{+}$ GV oocytes. (E, F) Scatter plot visualisation of DNA methylation (3-kb sliding windows, 1.5kb steps) for published GV WGBS data (Shirane et al., 2013) versus *Hira*$^{f/f}$ oocytes (E), and *Hira*$^{f/f}$ versus *Hira*$^{f/f}$, *Gdf9-Cre*$^{+}$ *oocyte* (F); Correlation value (R) is based on Pearson's test. (G) Quantification of DNA methylation at imprinted germline DMRs in *Hira*$^{f/f}$, and *Hira*$^{f/f}$, *Gdf9-Cre*$^{+}$ oocytes. (H) Quantification of DNA methylation at various repeat families in *Hira*$^{f/f}$, and *Hira*$^{f/f}$, *Gdf9-Cre*$^{+}$ oocytes. (I) Effects on DNA methylation in Hira deleted oocytes are more pronounced at highly expressed genes. DNA methylation was quantified for genes defined as high, median, low expressed based on our RNA-Seq data for each genotype. (J) Immunofluorescence staining of Triton pre-extracted GV oocytes. Note that Dnmt3a is chromatin associated in both *Hira*$^{f/f}$ and *Hira*$^{f/f}$, *Gdf9-Cre*$^{+}$ GV oocytes. (K) 3kb probes normally methylated in control oocytes (>80% methylation in *Hira*$^{f/f}$ oocytes) were binned according to their difference in DNA methylation between *Hira*$^{f/f}$ and *Hira*$^{f/f}$, *Gdf9-Cre*$^{+}$, CpG density of the probes was calculated and reported as a boxplot (***: $p<0.001$, Kruskall-Wallis test).

Supplemental Table Legends

Table S1. Summary of differential gene expression analysis between *Hira*$^{f/f}$ *Gdf9-Cre*$^{+}$ and *Hira*$^{f/f}$ MII oocytes, related to Figure 4.

The log fold change (LogFC), p-value (PValue), and false discovery rate (FDR) were computed by EdgeR software; the FPKM values for each gene for each sample were computed using HTSeq and custom R script.

Table S2. Summary of *de novo* transcript assembly using CuffCompare for *Hira*$^{f/f}$ *Gdf9-Cre*$^{+}$ and *Hira*$^{f/f}$ MII oocytes, related to Figure 5.

The transcript ID, transcript class, and FPKM for each transcript for each sample were computed using CuffCompare software.

Table S3. Summary of differential gene expression analysis between *Hira*$^{f/f}$ *Zp3-Cre*$^{+}$ and *Hira*$^{f/f}$ MII oocytes, related to Figure 4 and Figure S8.

The log fold change (LogFC), p-value (PValue), and false discovery rate (FDR) were computed by EdgeR software; the FPKM values for each gene for each sample were computed using HTSeq and custom R script.

Table S4. Summary of *de novo* transcript assembly using CuffCompare for *Hira*$^{f/f}$ *Zp3-Cre*$^{+}$ and *Hira*$^{f/f}$ MII oocytes, related to Figure 5 and Figure S8.

The transcript ID, transcript class, and FPKM for each transcript for each sample were computed using CuffCompare software.

Supplemental Experimental Procedures

Mice

Hira (*Hira*$^{f/f}$) mice were generated by the Wellcome Trust Sanger Institute (UK). Oocyte-specific Hira depletion was achieved by crossing *Hira*$^{f/f}$ mice with *Gdf9-iCre* (Lan et al., 2004) or with *Zp3-Cre* mice (de Vries et al., 2000) (obtained from Prof A. Surani, Cambridge, UK), respectively.

The *H3.3B-EGFP* knock-in mouse was generated in the MRC transgenic facility by standard protocol. The knock-in vector was provided by Prof R. Festenstein and transfected into E14 ES cells by electroporation. Positive ES clones were injected into C57B6-derived E3.5 blastocysts and implanted into 2.5 days post-coitum pseudo-pregnant female mice. Germline transmission was assessed by chimaerism in the pups.

Protamine 1-EGFP mice (Haueter et al., 2010) were re-derived and provided by Dr. P. Pelczar. All mutant mice strains were of C57B6 genetic background. All animal experiments were carried out under a UK Home Office Project Licence in a Home-Office designated facility.

In vitro fertilisation (IVF), *in vitro* maturation (IVM) and parthenogenesis

IVF and parthenogenesis were carried out as described previously (Nashun et al., 2010). Briefly, three weeks old mice were super-ovulated by intraperitoneal injection using 5 IU pregnant mare's serum gonadotropin (PMSG) and 5 IU of human chorionic gonadotropin (hCG) 48 hours later. For *in vitro* fertilization, the cumulus-oocyte complexes were transferred to HTF medium supplemented with 10 mg/ml BSA (Sigma-Aldrich) and inseminated with capacitated spermatozoa obtained from the caudal epididymides of adult B6CBAF1 male mice (Charles River or Harlan, UK). The spermatozoa capacitation was

achieved by pre-incubating for 2 h in HTF medium. Fertilized oocytes were washed in HTF and cultured in KSOM. Oocyte numbers were counted after digesting the cumulus-oocyte complexes with 0.3mg/ml hyaluronidase (Sigma-Aldrich), or four hours after insemination in the case of IVF.

Germinal vesicle (GV) stage oocytes were obtained from 3-week old females as described previously (Nashun et al., 2010). The ovaries were removed and transferred to M2 medium supplemented with 0.2 mM 3-isobutyl-1-methylxanthine (IBMX; Sigma-Aldrich). The ovarian follicles were punctured with a 26-gauge needle, and a narrow-pore glass pipette was used to remove the cumulus cells from the cumulus-oocyte complexes. For *in vitro* maturation, GV-oocytes were then transferred to α-minimal essential medium (Life Technologies,) containing 5% fetal bovine serum (FBS; Sigma-Aldrich), and 10 ng/ml epidermal growth factor (EGF; Sigma-Aldrich). Oocyte maturation was assessed by the first polar body extrusion after 16 hours incubation. Similarly, growing oocytes were collected from ovaries of 14 to 16 days old mice in M2 medium.

Immunofluorescence staining of mouse oocytes and zygotes

Oocytes and embryos were fixed for 20 minutes in PBS containing 4% paraformaldehyde (PFA) at room temperature and washed with 1% BSA/PBS three times unless otherwise stated. The cells were permeabilized by incubating in 1% BSA/PBS containing 0.5% Triton X-100 for 30 min at room temperature, and, after washing with 1% BSA/PBS three times, incubated with primary antibodies in 1% BSA/PBS containing 0.1% Triton X-100 overnight at 4ºC, washed three times, and incubated for 1 hour in the dark with Alexa Fluor 488- and/or 568-conjugated IgG secondary antibody (dilution 1:300, Molecular probes) in the same buffer. DNA was stained for 10 minutes with 3 μg/ml 4,6-diamidimo-2-phenylindole (DAPI) and the cells were then mounted either with Vectashield solution (Vector Laboratories) on

glass slides for single section imaging or with ProLong Gold mounting medium (Life Technologies) for sequential Z-stack imaging. Fluorescence was detected using a Leica TCS SP5 confocal microscope with a 63x objective and Z-step size of 0.5 μm in the case of Z-stack scanning. More than 12 oocytes/zygotes were examined in each immunofluorescence staining panel unless otherwise specified.

Primary antibody list:

Antibody target	Host	Supplier/Catalogue number	Dilution
Hira	Mouse	Millipore; #04-1488.	1:100
UBN1	Rabbit	Sigma-Aldrich; SAB4501346.	1:100
CABIN1	Rabbit	Abcam; Ab3349.	1:100
ATRX	Rabbit	Santa Cruz; SC-15408.	1:100
DAXX	Rabbit	Santa Cruz; SC-7152.	1:100
Pan histone	Mouse	Millipore; MAB3422.	1:100
H2A.X	Rabbit	Abcam; Ab11175.	1:100
γ-H2A.X	Mouse	Millipore; JBW301.	1:100
EGFP	Goat	Abcam; Ab5450.	1:200
Flag-epitope	Mouse	Sigma; F1804.	1:100
CENP-A	Rabbit	Cell Signalling; 2048.	1:100
H3K4me1	Rabbit	Abcam; AB8895.	1:200
H3K27me3	Rabbit	Cell Signalling; 9756.	1:400
H3K36me3	Rabbit	Abcam; AB9050.	1:400
Dnmt3a	Mouse	Imgenex; IMG268.	1:200
Dnmt3l	Mouse	Abnova; PAB2230.	1:100
EGFP	Goat	Abcam; AB5450.	1:100

5-methylcytosine (5mC) staining in oocytes and zygotes

The staining was carried out as described previously (Hajkova et al., 2010). Briefly, zygotes were fixed for 20min with 4% PFA and permeabilized for 40 min with 0.5% Triton X-100 in 1% BSA/PBS, treated with 10 mg/ml RNase A (Roche) in 1% BSA/PBS for 1 hour at 37^{o}C, and incubated in 4N HCl for 15 min at 37^{o}C to denature genomic DNA, followed by a 10 min wash in 1% BSA/PBS. After incubating for 30 min at room temperature in 1% BSA/PBS containing 0.1% Triton X-100, the cells were incubated with anti-5mC antibody (Diagenode, clone 33D3, 1:5000 dilution) at 4^{o}C overnight in the same buffer. Zygotes were subsequently

washed three times in 1% BSA/PBS containing 0.1% Triton X-100 for 10 min and incubated with Alexa Fluor 405-conjugated IgG secondary antibodies (dilution 1:300, Molecular Probes) for 1 hour in dark at room temperature. DNA was stained with propidium iodide (PI) (0.25mg/ml). After the final wash in 1% BSA/PBS for 30 min, the oocytes or zygotes were mounted in ProLong Gold mounting medium without DAPI (Life Technologies).

RNA preparation and RT-PCR analysis

Total RNA was purified using Trizol (Life Technologies). RNA from 20 zygotes was collected in 1ml Trizol in the presence of 10 pg of an exogenous RNA standard. Reverse transcription was performed using PrimeScript RT Reagent Kit with gDNA Eraser (Takara Bio, RR047A). cDNA corresponding to 2 zygotes was analysed using SensiMix SYBR No-ROX (Bioline) in a CFX96 real-time PCR detection system (Bio-Rad). Relative expression was normalized to exogenous standard and two-tailed unpaired t-test was performed. Primers:

Primer name	Sequence(5'-3')
Hira exon 1-3_F	AAGCTCTTGAAGCCAACCTG
Hira exon 1-3_R	GGCAAAGCATCTTGGGAATA
Hira exon 4-6_F	TTAGCTTCTGGGGGAGATGA
Hira exon 4-6_R	CATCACATCGCCTGAGTGAC
Hira exon 12_F	GCCGAATTCACCAGTCTACC
Hira exon 12_R	ACTTTCCCCATTGACCACAC

Detection of DNA replication and transcription in zygotes and oocytes

In order to detect DNA replication or general transcription, fertilized oocytes were transferred into medium containing 400uM of 5-ethynyl deoxyuridine (EdU, included in C10337, Life Technologies) 4 hours after insemination or 1mM of 5-ethynyl uridine (EU, included in C10329, Life Technologies) 6 hours after insemination, respectively. Zygotes were collected at 10 hours after insemination and zona pellucida was removed by Tyrode's acidic solution before fixation in PFA 4% for 20 min at room temperature. Growing or GV oocytes were

incubated for 4 hours with 400uM of EdU prior to fixation. EU or EdU staining was done according to manufacturer's instruction.

TUNEL assay detection of the DNase I sensitivity

Hira$^{f/f}$ or *Hira* mutant GV-oocytes were collected from siblings of the same litter as described above and pre-extracted immediately in ice-cold solution (50 mM NaCl, 3 mM $MgCl_2$, 0.5% Triton X-100, 300 mM sucrose in 25 mM HEPES pH 7.4) for 5 min. The oocytes were then incubated with different concentrations (0.1, 0.01or 0.001 U/μL) of DNase 1 (NEB) for 5 min at 37 ^{o}C in the same buffer without Triton X-100 and fixed for 10 min in 2% PFA/PBS at room temperature. TUNEL assay was done using Click-iT TUNEL Alexa Fluor Imaging Assay (Life Technologies, C10245) according to manufacturer's instructions.

***In vitro* mRNA synthesis and microinjection**

The cDNA sequence of human histone H3.1 (Dr. T. Bartke, MRC Clinical Sciences Centre) or H3.2, H3.3 (Prof. N.Dillon, MRC Clinical Sciences Centre) was subcloned into pGEM-T Easy Vector (Promega) and Flag-epitope tag was added at N-terminal tail by PCR amplification. Plasmids containing Flag-H2A.X and Flag-H4 were obtained from Prof.F.Aoki (University of Tokyo). *In vitro* mRNA synthesis and microinjections were performed as described previously (Nashun et al., 2010). Briefly, plasmids were linearized by appropriate restriction enzymes (NEB). 5'-capped mRNAs were synthesized using Sp6 or T7 mMessage mMachine kit (Ambion) and poly (A) tails were added by a Poly (A) Tailing Kit (Ambion). Finally, the DNA template was removed by Turbo DNase treatment and synthesized mRNA was extracted by phenol/chloroform extraction followed by isopropanol precipitation. Microinjection was performed under an inverted microscope (Eclipse TE200; Nikon) using a micromanipulator (Narishige) and microinjector (Medical System Pico-Injector PLI-100).

Approximately 10 pl synthetic RNA (~200 μg/ml) was microinjected into the cytoplasm of oocytes or embryos.

Haematoxylin & Eosin (H&E) staining of ovarian sections

Ovarian tissues were fixed in 4% paraformaldehyde overnight at 4 ^{o}C and embedded in O.C.T and stored at -80 ^{o}C before use. 10 μm sections were prepared using a Leica CM1950 cryomicrotome (Leica Microsystems). For H&E staining, the sections were air dried for several minutes to remove moisture and stained with filtered 0.1% Mayers Hematoxylin (Sigma-Aldrich, MHS-16) for 10 minutes. Then, rinsed in cool running water for 5 minutes in a Coplin jar and dipped in 0.5 Eosin Y (Sigma-Aldrich, E4009) for 12 times. The sections were dipped in distilled water until the eosin stopped streaking and successively moved through increasing concentrations of EtOH. (dipped 10 times each in 50% and 70% EtOH and equilibrated in 95% EtOH for 30 seconds and 100% EtOH for 1 minute). Xylene was used to replace the absolute alcohol and DPX (VWR, 360294H) was used for mounting. Digital images were obtained using a ZEISS Axiophot microscope with a 5x objective.

Single MII oocyte ATP measurement

Three weeks old *Hira*$^{f/f}$ or *Hira*$^{f/f}$ *GDF9-Cre*$^{+}$ siblings were superovulated and the cumulus-oocyte complexes were disassociated by hyaluronidase digestion. Single cell ATP measurement was conducted using ATPlite Luminescence Assay System (PerkinElmer) according to manufacturer's instructions.

Single cell RNA-Seq on *Hira*$^{f/f}$, *Hira*$^{f/f}$, *GDF9-Cre*$^{+}$ and *Hira*$^{f/f}$, *Zp3-Cre*$^{+}$ MII oocytes

cDNA synthesis and amplification was performed directly on single *Hira*$^{f/f}$, *Hira*$^{f/f}$ *Gdf9-Cre*$^{+}$ and *Hira*$^{f/f}$, *Zp3-Cre*$^{+}$ MII oocytes with the SMARTer Ultra Low Input RNA kit (Clontech). 0.5 uL of ERCC RNA spike-in mix 1 (Life Technologies), diluted 1:10^{5}, was

added to each reaction prior to cDNA synthesis. The amplified cDNA was fragmented by Covaris S2 sonicator (Covaris) and converted to sequencing libraries following the NEBNext DNA Library Prep (NEB) using the NEBNext Multiplex Oligos for Illumina (NEB). Bar-coded libraries were pooled and sequenced on two lanes of the Illumina HiSeq 2000 instrument. mRNA-seq reads were aligned to the mouse genome (mm9, NCBI build 37) with Bowtie v0.12.8/Tophat v2.0.2 (http://tophat.cbcb.umd.edu), which allows mapping across splice sites by reads segmentation. Annotations from Ensembl Gene version 67 were used as gene model with Tophat. Spike-in reads were aligned to ERCC spike-in sequences using bowtie2 with the following settings: -D 20 -R 3 -N 0 -L 20 -i S,1,0.50. For differential expression analysis, read counts per annotated gene were computed using HTSeq and expression level of each gene was quantified with FPKM (*Fragments Per Kilobase of Exon Per Million Fragments Mapped*) using R script. Differential expression analysis was performed using edgeR (version 3.1.10) and genes that showed significant differences at FDR < 0.1 between *Hira*$^{f/f}$ and *Hira*$^{f/f}$ *Gdf9-Cre*$^{+}$ (or between *Hira*$^{f/f}$ and *Hira*$^{f/f}$ *Zp3-Cre*$^{+}$) oocytes were identified. Gene ontology analysis of differentially expressed genes was performed with DAVID (http://david.abcc.ncifcrf.gov). For Gene Set Enrichment Analysis (version 2.0.7), the gene list was ranked based on the FDR (i.e. '1 – FDR') and fold-change (i.e. up-regulated genes were multiplied by a factor of '1'; down-regulated genes were multiplied by a factor of '-1') computed from edgeR differential expression analysis. To compare the gene expression changes between *Hira*$^{f/f}$ and *Hira*$^{f/f}$ *Gdf9-Cre*$^{+}$ (or between *Hira*$^{f/f}$ and *Hira*$^{f/f}$ *Zp3-Cre*$^{+}$) oocytes with expression changes over the course of oocyte development, we clustered previously published microarray expression data from primordial, primary, secondary, small antral and large antral follicle stages (Pan et al., 2005) using k-means clustering (n=8) and created a gene set for each cluster. Where multiple probes aligned to a single annotated gene, the mean expression value was used. For all tests, GSEA was carried out with default setting,

with the exception that the maximum gene set size was increased to 3000 genes. To determine the novel transcribed fragments that mapped entirely to intronic and intergenic regions of the mouse genome, mRNA-Seq reads were re-analysed with CuffCompare (version 2.1.1), which allows for the identification and classification of previously unannotated transcripts (Trapnell et al., 2010). The Gene Expression Omnibus (GEO) accession number for the *Hira*$^{f/f}$ *Gdf9-Cre*$^{+}$ and *Hira*$^{f/f}$, *Zp3-Cre*$^{+}$ single oocyte RNA-sequencing data is GSE66931 and GSE73382, respectively.

Single cell whole genome bisulphite sequencing and analysis on *Hira*$^{f/f}$ and *Hira*$^{f/f}$, *Gdf9-Cre* oocytes

To profile the DNA methylation landscape of *Hira*$^{f/f}$ and *Hira*$^{f/f}$, *Gdf9-Cre*$^{+}$ oocytes, we used a single cell bisulphite sequencing approach (scBS-Seq) that we had previously described (Smallwood et al., 2014). Briefly, MII oocytes were individually collected by mouth pipetting and lysed in a buffer containing 10mM Tris-Cl (pH 7.4), 1% SDS and 4U of Proteinase K. Bisulphite treatment was performed directly on the lysate using the Imprint DNA Modification kit (Sigma) (two-step protocol, incubation at 65 °C for 90 min, 95 °C for 3 min and 65 °C for 20 min), followed by depurination and purification of converted DNA using the PureLink PCR Micro kit (Life Technologies). First complementary strand synthesis was performed using Klenow exo- (50U, Sigma) and a biotinylated Illumina-based adapter with 9 random nucleotides for priming (biotin-CTACACGACGCTCTTCCGATCTNNNNNNNNN). This step was repeated an additional 4 times, with DNA denaturation (95 °C, 1min) in between. After capture of the neo-synthesised strands using streptavidin magnetic beads, second strand synthesis was performed using an Illumina-based adapter with 9 random nucleotides (TGCTGAACCGCTCTTCCGATCTNNNNNNNNN). Libraries were then amplified for 13 cycles using KAPA HiFi HotStart DNA Polymerase (KAPA Biosystems), Illumina PE1.0 oligo, and iPCR tag reverse oligos for indexing (Smallwood et al., 2014).

Libraries were purified using 0.8x AMPure XP beads (Agencourt) according to the manufacturer's guideline.

Libraries were assessed for quality and quantity using the Bioanalyser platform (Agilent) and the KAPA Library Quantification kit (KAPA Biosystems). For each genotype, 14 single cell libraries were pooled for sequencing (100-bp paired-end, HiSeq2500 rapid-run mode). Mapping of sequencing reads (NCBI37) and cytosine methylation extraction were performed using Bismark as previously described (Smallwood et al., 2014). The DNA methylation landscape of *Hira*$^{f/f}$ and *Hira*$^{f/f}$, *Gdf9-Cre*$^{+}$ oocytes were generated by merging all datasets from each genotype, as previously described (Smallwood et al., 2014). Data visualization and analysis were performed using SeqMonk, custom R and Java scripts.

For absolute DNA methylation quantification at the genome level or depending on the genomic contexts, individual cytosines (CpGs) were quantified (5reads cut-off). For intragenic, intergenic, exonic and intronic genomic contexts (Figure 6F), CpGs overlapping CpG islands were discarded. Promoters were defined by the genomic region (-1kbp, +200bp) surrounding annotated transcription start-sites, and CpG poor promoters were defined as promoters not overlapping CpG islands. For correlation with published oocytes whole genome bisulfite sequencing data (Shirane et al., 2013) (Figure 6C, S7E, S7I, DNA Data Bank of Japan accession number DRA000570), and for correlation with transcription, 3kb overlapping windows (1.5kb steps) were quantified for absolute level of methylation (probes defined as informative if at least 3 reads per CpGs and 7 informative CpGs per window). CGI methylation (including imprinted gDMRs) was determined by averaging individual CpGs (CpGs present in at least half of the single cells, and at least 5CpGs per CGI). The Gene Expression Omnibus (GEO) accession number for the *Hira*$^{f/f}$ and *Hira*$^{f/f}$ *Gdf9-Cre*$^{+}$ single cell bisulphite sequencing data is GSE66629.

Detection of 5-methylcytosine by ultra-sensitive LC-MS

Genomic DNA from oocytes was extracted using ZR-Duet DNA/RNA Miniprep kit (Zymo Reasearch) following manufacturer instructions and eluted in LC/MS grade water. DNA was digested to nucleosides using a digestion enzyme mix provided by NEB. A dilution-series made with known amounts of synthetic nucleosides and the digested DNA were spiked with a similar amount of isotope-labelled nucleosides (provided by T. Carell, LMU Munich) and separated on an Agilent RRHD Eclipse Plus C18 2.1 × 100 mm 1.8u column by using the UHPLC 1290 system (Agilent) and an Agilent 6490 triple quadrupole mass spectrometer. To calculate the quantity of individual nucleosides, standard curves representing the ratio of unlabelled over isotope-labelled nucleosides were generated and used to convert the peak-area values to corresponding quantity. Threshold for quantification is a signal-to-noise (calculated with a peak-to-peak method) above 10.

Supplemental References

de Vries, W.N., Binns, L.T., Fancher, K.S., Dean, J., Moore, R., Kemler, R., and Knowles, B.B. (2000). Expression of Cre recombinase in mouse oocytes: A means to study maternal effect genes. Genesis *26*, 110-112.

Hajkova, P., Jeffries, S.J., Lee, C., Miller, N., Jackson, S.P., and Surani, M.A. (2010). Genome-wide reprogramming in the mouse germ line entails the base excision repair pathway. Science *329*, 78-82.

Haueter, S., Kawasumi, M., Asner, I., Brykczynska, U., Cinelli, P., Moisyadi, S., Burki, K., Peters, A.H., and Pelczar, P. (2010). Genetic vasectomy-overexpression of Prm1-EGFP fusion protein in elongating spermatids causes dominant male sterility in mice. Genesis *48*, 151-160.

Lan, Z.J., Xu, X., and Cooney, A.J. (2004). Differential oocyte-specific expression of Cre recombinase activity in GDF-9-iCre, Zp3cre, and Msx2Cre transgenic mice. Biol Reprod *71*, 1469-1474.

Nashun, B., Yukawa, M., Liu, H., Akiyama, T., and Aoki, F. (2010). Changes in the nuclear deposition of histone H2A variants during pre-implantation development in mice. Development *137*, 3785-3794.

Pan, H., O'Brien M, J., Wigglesworth, K., Eppig, J.J., and Schultz, R.M. (2005). Transcript profiling during mouse oocyte development and the effect of gonadotropin priming and development in vitro. Dev Biol *286*, 493-506.

Shirane, K., Toh, H., Kobayashi, H., Miura, F., Chiba, H., Ito, T., Kono, T., and Sasaki, H. (2013). Mouse Oocyte Methylomes at Base Resolution Reveal Genome-Wide Accumulation of Non-CpG Methylation and Role of DNA Methyltransferases. PLoS Genet *9*.

Smallwood, S.A., Lee, H.J., Angermueller, C., Krueger, F., Saadeh, H., Peet, J., Andrews, S.R., Stegle, O., Reik, W., and Kelsey, G. (2014). Single-cell genome-wide bisulfite sequencing for assessing epigenetic heterogeneity. Nat Methods *11*, 817-820.

Trapnell, C., Williams, B.A., Pertea, G., Mortazavi, A., Kwan, G., van Baren, M.J., Salzberg, S.L., Wold, B.J., and Pachter, L. (2010). Transcript assembly and quantification by RNA-Seq reveals unannotated transcripts and isoform switching during cell differentiation. Nat Biotechnol *28*, 511-515.